Tracing the migration of mantle CO_2 in gas fields and mineral water springs in south-east Australia using noble gas and stable isotopes

Rūta Karolytė[1*], Gareth Johnson[1], Domokos Györe[2], Sascha Serno[1], Stephanie Flude[1], Finlay M. Stuart[2], Allan R. Chivas[3,4], Adrian Boyce[2] and Stuart M.V. Gilfillan[1]

[1] School of GeoSciences, University of Edinburgh, James Hutton Road, Edinburgh, EH9 3FE, UK

[2]Isotope Geoscience Unit, Scottish Universities Environmental Research Centre (SUERC), East Kilbride, G75 0QF, UK

[3]GeoQuEST Research Centre, School of Earth and Environmental Sciences, University of Wollongong, Wollongong, NSW 2522, Australia

[4]Department of Earth Sciences and Sprigg Geobiology Centre, The University of Adelaide SA 5005, Australia

*Author for correspondence: ruta.karolyte@ed.ac.uk

Keywords: Carbon Capture and Storage; geochemical tracing; noble gases; carbon isotopes; helium; mantle; CO_2 springs; solubility fractionation; Otway Basin.

Abstract

Geochemical monitoring of CO_2 storage requires understanding of both innate and introduced fluids in the crust as well as the subsurface processes that can change the geochemical fingerprint of CO_2 during injection, storage and any subsequent migration. Here, we analyse a natural analogue of CO_2 storage, migration and leakage to the atmosphere, using noble gas and stable isotopes to constrain the effect of these processes on the geochemical fingerprint of the CO_2. We present the most comprehensive evidence to date for mantle-sourced CO_2 in south-east Australia, including well gas and CO_2-rich mineral spring samples from the Otway Basin and Central Victorian Highlands (CVH). $^3He/^4He$ ratios in well gases and CO_2 springs range from 1.21 to 3.07 R_A and 1.23 – 3.65 R_C/R_A, respectively. We present chemical fractionation models to explain the observed range of $^3He/^4He$ ratios, He, Ne, Ar, Kr, Xe concentrations and $\delta^{13}C(CO_2)$ values in the springs and the well gases. The variability of $^3He/^4He$ in the well gases is controlled by the gas residence time in the reservoir and associated radiogenic ^4He accumulation. $^3He/^4He$ in CO_2 springs decrease away from the main mantle fluid supply conduit. We identify one main pathway for CO_2 supply to the surface in the CVH, located near a major fault zone. A new solubility fractionation model, describing noble gas partitioning between water and gas at the shallow surface during bubble formation, is proposed to explain the range in noble gas concentrations and $\delta^{13}C(CO_2)$ values measured in the mineral spring samples. This process is also responsible for low ^3He concentrations and associated high $CO_2/^3He$, which are commonly interpreted as evidence for mixing with crustal CO_2. The elevated $CO_2/^3He$ can be explained solely by solubility fractionation without the need to invoke other CO_2 sources. The noble gases in the springs and well gases can be traced back to a single end-member which has

suffered varying degrees of radiogenic helium accumulation and late stage degassing. This work shows that combined stable and noble gas isotopes in natural gases provide a robust tool for identifying the migration of injected CO_2 to the shallow subsurface.

1. Introduction

The development of geochemical tracing techniques to ascertain the origin and genetic link between natural gases trapped in subsurface reservoirs and those degassing at the surface is important to the safe and successful deployment of carbon capture and storage (CCS). Safe disposal of captured industrial CO_2 requires verification of the fate of the injected gas and reassurance that injected gas does not migrate to the surface (IPCC, 2005). To ensure this, CCS operators have to adhere to legislative guidelines and verify that injected CO_2 is securely contained within the reservoir formation (Dixon et al., 2015). While a variety of geophysical, geoelectric and thermal sensing monitoring techniques exist (Giese et al., 2009), the high sensitivity of geochemical monitoring techniques is useful for detecting seepage at low concentrations, verifying gas origin and tracing the interactions between different crustal fluids (Myers et al., 2013; Stalker and Myers, 2014; Roberts et al., 2017).

The noble gas isotopes have previously been applied in an engineered setting to assess CO_2 migration, dissolution and residual trapping in reservoir pore spaces at the Cranfield CO_2-EOR site field (Györe et al., 2015; Györe et al., 2017) and to study industrial underground natural gas storage in the Paris Basin (Jeandel et al., 2010). Noble gas tracers have been used to refute allegations of injected CO_2 leakage to the surface near the Weyburn-Midale CO_2 Monitoring and Storage Project (Gilfillan et al., 2017) and to identify fugitive gas migration to shallow aquifers caused by industrial hydraulic fracturing operations (Darrah et al., 2014). The techniques used in these industrial studies have been informed by preceding research of natural gas fields and springs (e.g. Ballentine and O'Nions, 1994; Gilfillan et al., 2014, 2009, 2008; Sherwood Lollar et al., 1997; Wilkinson et al., 2009). Natural analogue studies remain a crucial gateway to developing geochemical tracing methods for the industrial sector, providing information about fluid migration and retention processes occurring over geological time scales (Baines and Worden, 2004; Haszeldine et al., 2005; Holland and Gilfillan, 2013).

Helium is an unrivalled indicator of crustal fluid migration in the subsurface because it is sensitive to changes in the balance between volatiles derived from the mantle and the crust. This is because the original helium composition of any subsurface fluid is not significantly modified by interaction with groundwater due to the low abundance of helium in the atmosphere (Ozima and

69 Podosek, 2002). Hence, helium is particularly applicable to tracing gas migration through a water
70 system in both natural and industrial fugitive gas migration monitoring settings. Here we draw from
71 existing methodologies of helium use in tracing the migration of mantle fluids (Sano et al., 1990;
72 Sakamoto et al., 1992), mixing of different fluid sources (O'Nions and Oxburgh, 1988; Sano and
73 Marty, 1995) and dating natural gas and groundwater resources (Zhou and Ballentine, 2006; Liu et
74 al., 2016) to provide a comprehensive account on the geochemical link between natural CO_2 gases,
75 trapped in the subsurface and emanating in the shallow surface.

76 Noble gases are soluble in water and partition according to their relative solubilities during
77 gas-water equilibration. This property has been utilised mainly in assessing reservoir-scale water-gas
78 equilibration and gas migration or groundwater recharge conditions (Bosch and Mazor, 1988;
79 Ballentine et al., 1996; Barry et al., 2016) and the presence of 'excess air' above the atmospheric
80 solubility equilibrium (Aeschbach-Hertig et al., 2008; Kipfer et al., 2002). The former is largely based
81 on atmospheric noble gas ratios, whilst the latter combines ratios with elemental concentrations.
82 Atmospheric noble gas ratios in CO_2 springs are commonly similar to air saturated water (ASW) and
83 the utility of these noble gases is often overlooked. We discuss the use of noble gas concentration
84 data in assessing the solubility fractionation effects of near-surface degassing and reconstructing the
85 original noble gas composition for the purpose of tracing.

86 The physical and chemical processes contributing to and modifying the noble gas contents of
87 CO_2 are explored using the data from three natural CO_2 fields in the Otway Basin of SE Australia and
88 ten natural CO_2-rich springs in Victoria. We focus on identifying the origin of the gases and the
89 genetic link between gases stored in reservoir traps and those emanating at the surface from the
90 natural mineral springs.

91 # 2 Geological setting

92 ## 2.1 Basin setting and location of CO_2 gas fields and springs

93 The Otway Basin developed along the southern Australian margin as a result of crustal
94 extension due to sea floor spreading between Australia and Antarctica. The sedimentary section of
95 the basin comprises Upper Jurassic – Lower Cretaceous Otway Group sediments (Bernecker and
96 Moore, 2003). The present geometry of the basin is characterised by NW-SE trending normal faults,
97 and was established during Jurassic to Cretaceous rifting and subsequent reactivation during a short-
98 lived period of basin inversion in the Miocene (Cox et al., 1995; Teasdale et al., 2003).

The basement comprises Lachlan and Delamerian fold belts, separated by the Moyston lithospheric suture which extends to the Moho (Fig. 1a). Parallel N-S trending large-scale shear zones and reverse faults connect to the Moyston Fault at depth (Fig. 1d) (Cayley et al., 2011). The structure of the Otway Basin has been strongly controlled by the fabric of the underlying basement. Old basement structures have a significant rheology contrast along them and are more likely to undergo structural reactivation during a change in the stress regime (Hand and Sandiford, 1999). The Jurassic-Cretaceous extension was mainly accommodated along structural weaknesses of the basement, which created graben and half-graben structures favourable for fluid trapping. Hydrocarbons and CO_2 discoveries in the Otway Basin therefore tend to coincide with the location of deep basement faults (Bernecker and Moore, 2003).

The basin contains numerous accumulations of CO_2, methane and other hydrocarbons in varying concentrations (Boult et al., 2004). The three gas fields investigated in this work contain CO_2 concentrations above 75 mol %, with the remainder of the gas content being primarily methane. The Caroline field is located in South Australia, near Mt Gambier and is a commercially explored CO_2 field which has a CO_2 concentration in excess of 98 % (Chivas et al., 1987). Boggy Creek and Buttress fields are located in the Port Campbell Embayment at the eastern side of the Otway Basin (Boreham et al., 2011). Methane generation is dated to mid-Paleogene (Duddy, 1997), followed by a later-stage CO_2 emplacement (Boult et al., 2004; Watson et al., 2004; Lyon et al., 2005).

CO_2-rich mineral spring waters emanate at the ground surface within the extent and north of the basin. Over a hundred ambient temperature mineral springs are located in the Central Victorian Highlands (CVH) (Fig. 1b). Mineral water flows through a fracture-dominated aquifer consisting of Ordovician low-grade metasedimentary sequence and discharges into topographic lows such as streambeds. Many of the springs also release CO_2 and can be identified as degassing CO_2 bubble trails into creek beds or standing pools of water. Springs are clustered along the Muckleford Fault, which is a deep Proterozoic reverse fault extending down to the lower crust and connecting to the Moyston suture zone (Cayley et al., 2011) (Fig. 1d).

Mineral springs also emerge on the northern coast of Bellarine Peninsula, at Clifton Springs near Geelong, on the south-eastern edge of the Otway Basin (Fig. 1c). The central part of the Bellarine Peninsula has been uplifted in the late Miocene during the inversion of NE-SW trending normal faults (Coulson, 1933). The north coast of the peninsula is structurally controlled by the Curlewis Monocline, underlain by a south dipping normal fault. The Curlewis Monocline is parallel to the structural lineaments of the basement and could be associated with deeper basement faults (Dahlhaus, 2003). CO_2 springs emerge along the shoreline parallel to the fault.

The basement and the Otway Basin are overlain by the Newer Volcanic Province (NVP) extrusives that stretch from the CVH to the northern edges of the Port Campbell Embayment. The province is a well preserved intra-plate basaltic lava field with more than 400 eruptive centres (Boyce, 2013), active between 5 Ma and 4.5 ka (Cas et al., 2017). The last eruption dated at 4.5 ka, occurred at Mount Gambier, located near the Caroline CO_2 field (Robertson et al., 1996). Many of the oldest eruptive centres are found in the eastern side of the province and near the CVH (4.6 - 2.6 Ma) (Price et al., 1997), but no systematic pattern of eruptions ages exists (Cas et al., 2017). There is no evidence for volcanic activity of this period in the Bellarine Peninsula where Clifton Springs are located, although The Older Volcanics (39 - 49 Ma) crop out in the area (Price et al., 1997). The cause of the recent volcanism is currently unresolved. Common theories include a mantle plume (Wellman and McDougall, 1974; Wellman, 1983), edge-driven isolated mantle convection (King and Anderson, 1998), batch-melting caused by fault reactivation (Lesti et al., 2008), or a combination of all these factors (Demidjuk et al., 2007; Davies and Rawlinson, 2014).

2.2 Previous noble gas studies of the gas fields and CO_2 springs

Despite the commercial exploration of CO_2 gas fields in the Otway Basin and springs in the CVH, studies of the CO_2 origins have been limited and the processes associated with the gas migration in the subsurface and to the surface are poorly understood. Chivas et al. (1987) reported $^3He/^4He$ values of up to 3.1 R_A in the Caroline field and Caffee et al. (1999) identified the presence of primordial Xe in the field, providing evidence for a mantle source. Mantle helium has also been reported in the Lavers-1 gas field in the Otway Basin (1.68 R/R_A) (Watson et al., 2004). Preliminary $^3He/^4He$ measurements of up to 3.1 R_A have been reported in CO_2 springs at the CVH (Chivas et al., 1983) but no further study has been published. It has been suggested that the source of mantle volatiles in CO_2 springs is associated with the NVP (Lawrence, 1969), however no conclusive evidence currently exists other than geographic proximity to the eruptive centres. Prior to this work no geochemical study into the origin of the CO_2 degassing at the Bellarine Peninsula had been published.

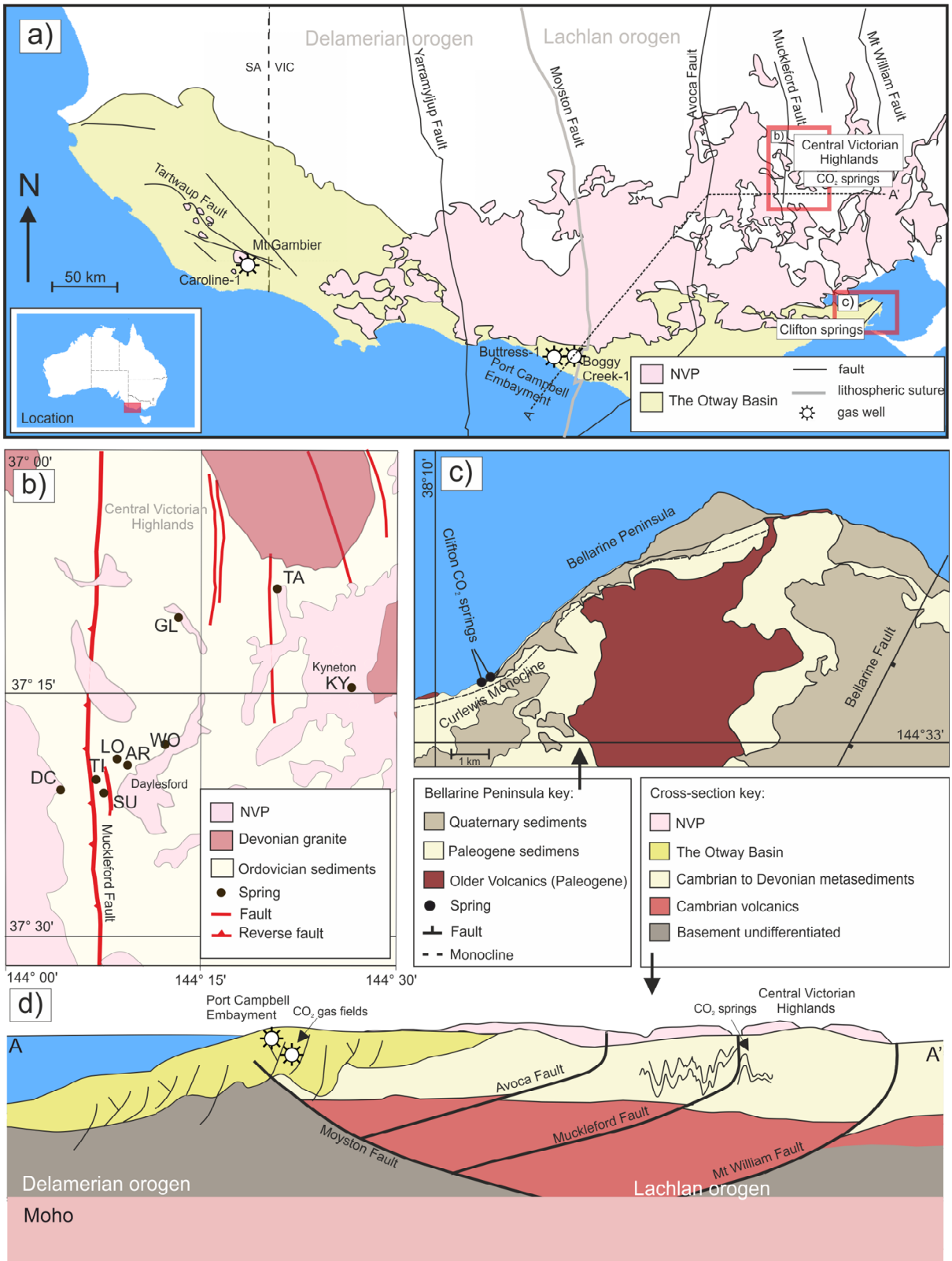

Figure 1. Location map of the studied CO_2 gas fields and springs. a) Studied well gases are in two localities in the Otway Basin: Port Campbell Embayment and Mt Gambier. Clifton Springs are located on the eastern edge of the basin. The CVH CO_2 springs emerge from the Ordovician basement rocks in the CVH. The Otway Basin and CVH are dissected by N-S trending faults. The Newer Volcanic province extends across both areas. b) Location of sampled CO_2 springs in CVH;

many of the springs are located near the Muckleford Fault (see Table 1 for sample name abbreviations). c) Clifton Springs are located on the coast of Bellarine Peninsula, along the crest of the Curlewis Monocline. d) Sketch cross-section (not to scale) of A-A' transect on Fig. 1a, showing the structural relationship between the basement and the basin. The Moyston and Mt Williams Faults extend to the Moho. Many of the basement faults (including The Muckelford fault at CVH) are inferred to be connected to the Moyston Fault at depth. Elements of the figure adapted from (Cartwright et al., 2002; Bernecker and Moore, 2003; Watson et al., 2003; Cayley et al., 2011; Cas et al., 2017)**.**

2. Methods

2.1 CO_2 sampling

Gas samples from the natural gas fields in the Otway Basin were collected directly from producing well heads, using 9.5 mm diameter refrigeration grade copper tubing connected to a pressure regulator by plastic hosing. Bubbling gases from the springs were collected using an inverted plastic funnel placed over a bubbling vent, placed into the water column to form an air-tight seal, allowing gas to flow through plastic hose to the copper tube. Tubes were purged for 5 minutes and sealed using two steel clamps specifically manufactured for the purpose of creating a helium leak-tight cold weld seal (Holland and Gilfillan, 2013). Mineral spring water samples were collected via hand pumps, filtered through 0.45 mm pore-size filters and filled into Nalgene bottles. The temperature, pH and TDS of the water in boreholes was measured in the field using a Hanna Instruments HI991300 Portable Waterproof temperature/pH/EC Meter with an accuracy of ± 0.5 °C, ± 0.01 pH and ± 1 µS/cm for temperature, pH and electrical conductivity respectively. TDS values were obtained from EC measurements using a conversion factor of 0.7 (Walton, 1989).

2.2 Laboratory procedures

All laboratory work was undertaken at the Scottish Universities Environmental Research Centre (SUERC). Copper tube samples were connected to an all-metal vacuum line, purified using VG Scienta ST22 titanium sublimation pump and ZrAl alloy getter. The isotopic composition of noble gases was measured using a MAP 215-50 mass spectrometer using techniques outlined in Györe et al. (2015). Bulk gas concentrations were measured using a Pfeiffer Vacuum QMS 200 quadrupole mass spectrometer and Hewlett Packard 5890 Series 11 Gas Chromatograph with uncertainties of ±1 %. $\delta^{13}(CO_2)$ values were determined using a VG Optima dual inlet isotope ratios mass spectrometer in dynamic mode using an internal standard (Györe et al., 2015). Values are reported relative to VPDB standard with uncertainties of ±0.2 ‰.

3. Results

A total of three well gas and ten spring samples were measured. Sample location, bulk gas composition, $\delta^{13}(CO_2)$ values, temperature, pH and TDS measurements are reported in Table 1. He, Ne and Ar isotope ratios, and He, Ne, Ar, Kr, Xe concentrations are reported in Table 2. The full suite of noble gases was measured in six of the CO_2 spring samples, while He isotopes were only measured in three well gas and four CO_2 spring samples.

Table 1. Details of the geographic location, bulk gas composition, $\delta^{13}(CO_2)$ values of 3 well gases and 10 CO_2 springs; pH, temperature and TDS measured in water from 10 mineral water bores.

Sample name		Location			Bulk gas composition*						$\delta^{13}C(CO_2)$ VPDB	Borehole water		
	Label	Region	Latitude	Longitude	CO_2	CH_4	C_2H_6	C_3H_8	C_4H_{10}	N_2		pH	T °C	TDS g/L
Well gases														
Caroline-1	**CA**	Mount Gambier, SA	-37.9417	140.9083	99	0.9	0.01	–	–	0.4	-4.1	–	–	–
Boggy Creek-1	**BC**	Port Campbell, VIC	-38.5261	142.8245	87	10.0	0.1	0.03	0.01	2.3	-5.6	–	–	–
Buttress-1	**BU**	Port Campbell, VIC	-38.5167	142.8084	77	19.7	0.8	1.1	–	1.9	-7.6	–	–	–
CO_2 springs														
Taradale	**TA**	CVH	-37.1393	144.3500	>99						-9.4	6.1	20.9	2.9
Locarno	**LO**	CVH	-37.3113	144.1412	>99						-7.2	6.1	16.7	1.6
Deep Creek	**DC**	CVH	-37.3419	144.0733	>99						-8.2	5.6	15.7	0.6
Glenluce	**GL**	CVH	-37.1623	144.2225	>99	0.1					-7.8	6.3	16.7	2.2
Woolnoughs	**WO**	CVH	-37.2942	144.2065	>99						-6.9	6.2	21.1	1.6
Clifton Springs	**CL**	Bellarine Peninsula	-38.1510	144.5659	>99						-6.0	5.5	20.5	3.8
Sutton	**SU**	CVH	-37.3480	144.1317	>99						-8.4	6.0	19.7	1.1
Argyle	**AR**	CVH	-37.3141	144.1553	>99						-9.2	5.8	15.1	1.0
Kyneton	**KY**	CVH	-37.2358	144.4200	>99						-8.0[a]	6.1	18.3	1.2
Tipperary	**TI**	CVH	-37.3391	144.1186	>99						-7.1	6.3	16.5	2.2

* Bulk gas composition for Caroline-1 from Chivas et al. (1987), Boggy Creek-1 from Akbari (1992)

[a] from Cartwright et al. (2002)

Table 2. Noble gas concentrations and isotopic ratios for 3 well gas samples and 10 CO_2 springs.

Sample name	$^{3}He/^{4}He$ (R_C/R_A)		$^{20}Ne/^{22}Ne$		$^{21}Ne/^{22}Ne$		$^{40}Ar/^{36}Ar$		$^{38}Ar/^{36}Ar$		$^{4}He \times 10^{-6}$		$^{20}Ne \times 10^{-9}$		$^{40}Ar \times 10^{-5}$		$^{84}Kr \times 10^{-9}$		$^{132}Xe \times 10^{-10}$	
Well gases																				
Caroline-1	3.07	(0.12)	–		–		–		–		96.0	(5.0)	2.2	(0.1)	–		–		–	
Boggy Creek-1	1.21	(0.01)	–		–		–		–		384.4	(18.6)	124.1	(5.3)	–		–		–	
Buttress-1	1.25	(0.01)	–		–		–		–		478.8	(23.2)	15.4	(0.7)	–		–		–	
CO_2 springs																				
Taradale	1.23	(0.03)	9.73	(0.06)	0.030	(0.001)	314	(1)	0.195	(0.008)	4.0	(0.2)	34.3	(1.5)	5.3	(0.2)	8.2	(0.3)	6.9	(0.4)
Locarno	3.14	(0.09)	9.68	(0.05)	0.030	(0.001)	303	(1)	0.191	(0.003)	5.7	(0.2)	59.1	(2.5)	7.8	(0.3)	10.4	(0.43)	6.5	(0.3)
Deep Creek	2.45	(0.07)	9.92	(0.05)	0.029	(0.001)	301	(5)	0.190	(0.003)	8.9	(0.4)	132.3	(5.6)	22.8	(0.8)	39.5	(1.6)	30.4	(1.6)
Glenluce	1.57	(0.07)	9.71	(0.05)	0.028	(0.000)	308	(1)	0.189	(0.003)	163.0	(6.0)	1372	(58)	94.4	(3.5)	63.1	(2.6)	25.6	(1.3)
Woolnoughs	1.71	(0.07)	9.78	(0.06)	0.030	(0.001)	299	(1)	0.190	(0.003)	0.97	(0.04)	1781	(3.7)	86.0	(3.2)	79.9	(3.3)	36.1	(1.9)
Clifton Springs	1.97	(0.06)	9.73	(0.06)	0.029	(0.001)	323	(1)	0.191	(0.003)	42.0	(2.0)	128.8	(5.5)	22.9	(0.8)	29.8	(1.2)	19.9	(1.0)
Sutton	3.14	(0.03)	–		–		–		–		1.61	(0.05)	42.5	(1.5)	–		–		–	
Argyle	3.65	(0.08)	–		–		–		–		87.9	(2.6)	5502	(196)	–		–		–	
Kyneton	1.24*	(0.04)	–		–		–		–		4.9	(0.1)	13834	(493)	–		–		–	
Tipperary	2.70	(0.05)	–		–		–		–		0.48	(0.01)	438.3	(8.9)	–		–		–	

Concentrations are in $cm^3(STP)/cm^3$.

Errors are 1σ standard deviation.

* $^{3}He/^{4}He$ reported uncorrected for atmospheric component due to air contamination

3.1. Bulk gas concentrations, $\delta^{13}(CO_2)$ and water measurements

The concentration of CO_2 in the Buttress field is 77 % with the remainder of gas predominately constituting of CH_4 (19.7 %), N_2 (1.9 %) and traces of higher hydrocarbons (0.8 % C_2H_6, 1.1 % C_3H_{10}). Bulk gas compositions for the other two well gases are taken from the literature. CO_2 concentration in the adjacent Boggy Creek field is slightly higher (87%) (Akbari, 1992). The Caroline field has the highest CO_2 concentrations of 99 % with traces of CH_4, N_2 and C_2H_6 (Chivas et al., 1987). All mineral spring gas samples were measured to be above 99 % CO_2 with the remainder of gas composed of noble gases. Glenluce is the only spring showing trace amounts of CH_4 (0.1 %). The $\delta^{13}(CO_2)$ values of the gas samples range from -9.4 to -6 ‰ in springs, and -7.6 to -4.1 ‰ in the well gases. The temperature of the water samples varies from 15.1 – 20.9 °C, pH ranges from 5.8 to 6.3 in CVH springs and 5.5 in Clifton Springs. TDS values range from 0.63 to 2.85 g/L.

3.2. Helium and $CO_2/^3He$ ratios

$^3He/^4He$ ratios are reported normalised to the value of air (where 1 R_A is the atmospheric ratio of 1.4×10^{-6}). $^3He/^4He$ R_c/R_A are corrected for ^4He derived from the atmospheric component, using the $^4He/^{20}Ne$ value of the sample following the methodology in Craig (1978). It is assumed that all ^{20}Ne is derived from ASW and the $^4He/^{20}Ne$ value of ASW at 20 °C is 0.27 (Kipfer et al., 2002). $^4He/^{20}Ne$ ratios of the well gases are 4-5 orders of magnitude above the ASW value (3097-44656) and range between 0.35 and 326 in the spring samples. $^3He/^4He$ R_c/R_A values differ significantly from the measured $^3He/^4He$ ratios in spring samples with $^4He/^{20}Ne$ ratios <10 (Woolnoughs and Tipperary). Kyneton is the only sample with significant atmospheric contamination ($^4He/^{20}Ne$ = 0.35) which would make the correction erroneous (Sano et al., 2006) therefore its $^3He/^4He$ value is reported uncorrected (1.24 R_A). The $^3He/^4He$ ratios of the remaining spring samples range from 1.23 to 3.65 Rc/R_A. $^3He/^4He$ ratios of well gases from the Port Campbell region are 1.21 and 1.25 R_A. The sample collected from the Caroline CO_2 field in South Australia exhibits a higher value of 3.07 R_A, in agreement with previous measurements (Chivas et al., 1987). All samples are compatible with two-component mixing in a $^3He/^4He$ vs $^4He/^{20}Ne$ plot, where variable $^3He/^4He$ end-members mix with ASW (Fig. 2).

$CO_2/^3He$ ratios of the well gases are within or below the Mid-Ocean Ridge Basalt (MORB) range of 1×10^9 to 1×10^{10} (Marty and Jambon, 1987). This is quite distinct from the higher $CO_2/^3He$ values predicted for near ^3He-free carbonates (O'Nions and Oxburgh, 1988; Sherwood Lollar et al., 1997). CO_2 concentrations in the spring samples are uniform, whilst $CO_2/^3He$ ratios vary over two orders of magnitude, 2.26×10^9 and 6.5×10^{11}, across the typical mantle and crustal values (Fig. 3).

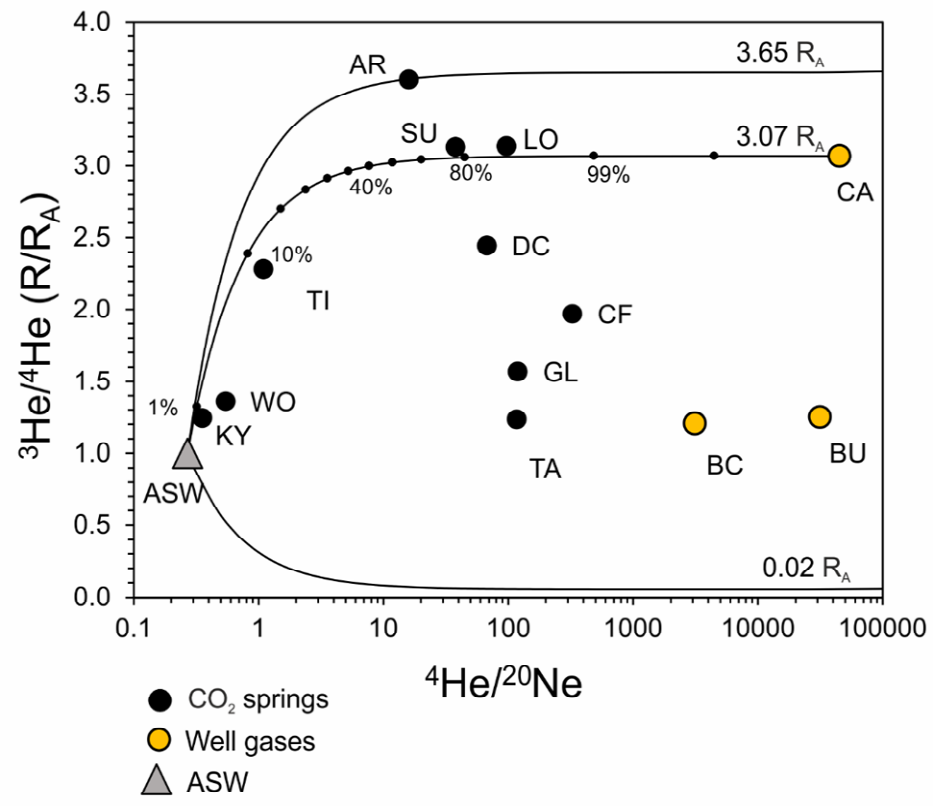

239

240 **Figure 2. $^3He/^4He$ R_A plotted against $^4He/^{20}Ne$ ratios of springs and well gases. Solid lines depict binary**
241 **mixing between ASW and the highest regional mantle end-member (Argyle, 3.65 R_A), Caroline field and a**
242 **crustal end-member (0.02 R/R_A). Black tick marks show percentage of helium from Caroline end-member in**
243 **the mixture. Few springs fall close to the mixing line with the Caroline field, the remaining samples have**
244 **variable amounts of crustal component. Errors are smaller than the symbols. Abbreviations of sample**
245 **names are given in Table 1. Abbreviations of sample names are given in Table 1.**

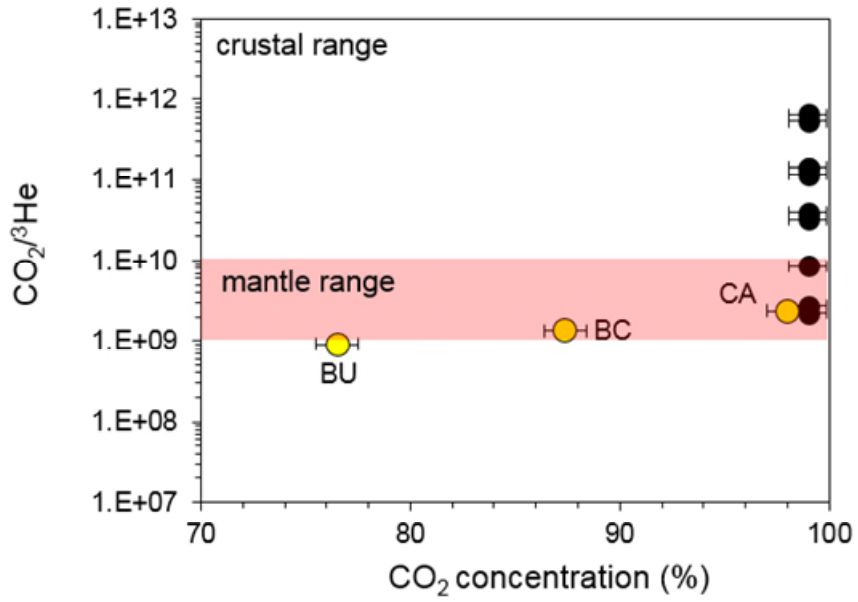

246

Figure 3. $CO_2/^3He$ ratios plotted against CO_2 concentrations for the well gases (yellow circles) and CO_2 springs (black circles). Vertical errors are smaller than the symbols. The shaded area shows the range of $CO_2/^3He$ values measured in mantle source volatiles (Marty and Jambon, 1987). $CO_2/^3He$ ratios above 1 x 10^{10} are typically associated with a crustal CO_2 source (O'Nions and Oxburgh, 1988). Well gas samples are within the mantle range but with positive correlation between $CO_2/^3He$ ratios and CO_2 concentrations. CO_2 concentrations are uniform in the spring samples, however $CO_2/^3He$ ratios are wide-ranging across the typical mantle and crustal values. Vertical errors are smaller than symbols. Abbreviations of sample names are given in Table 1.

Neon, argon, krypton and xenon concentrations were measured in six CO_2 spring samples (Taradale, Locarno, Deep Creek, Glenluce, Woolnoughs and Clifton Springs) (Table 2). $^{20}Ne/^{22}Ne$ ratios of the spring samples range between 9.68 and 9.92, close the air value of 9.8 (Ballentine, 1997). $^{40}Ar/^{36}Ar$ ratios range from 299 to 314, slightly above the value of air (298.5) (Ozima and Podosek, 2002). In contrast to relatively uniform and air-like isotope ratios, noble gas concentrations are highly variable. ^{20}Ne concentrations vary over three orders of magnitude ($3.4 \pm 1.5 \times 10^{-8}$ to $1.4 \pm 0.1 \times 10^{-5}$); ^{40}Ar concentrations vary from $5.3 \pm 0.2 \times 10^{-5}$ to $2.3 \pm 0.1 \times 10^{-4}$. Krypton and xenon concentrations range from $8.3 \pm 0.3 \times 10^{-9}$ to $1 \pm 0.04 \times 10^{-8}$ and $6.9 \pm 0.4 \times 10^{-10}$ to $3.6 \pm 0.2 \times 10^{-9}$, respectively.

4. Discussion – link between the CO_2 source in the reservoirs and springs

4.1. He-CO_2 abundance system

The trends in He-CO_2 abundance of well gases and CO_2 springs can be distinguished using a ternary diagram after Giggenbach et al. (1993). This allows depiction of the relative ratios between CO_2-^3He-^4He rather than absolute concentrations (Fig. 4). The MORB end-member (Marty and Jambon, 1987) is displayed for reference with a straight mixing line showing addition of radiogenic ^4He. Caroline, Buttress, and Boggy Creek well gases as well as Argyle and Glenluce springs fall on a mixing line between MORB and crustal end-members. The rest of the springs lie on the mixing trajectory with low He/high CO_2 end-member (the CO_2 apex of the plot).

Based on the observed trends, two main processes can be identified. Addition of radiogenic ^4He to the MORB-type component lowers the $^3He/^4He$, decreases $CO_2/^4He$ and does not affect $CO_2/^3He$ ratio (the trend towards the ^4He apex of the graph). All CO_2 well gas and spring samples exhibit variation in $^3He/^4He$ ratios due to radiogenic ^4He addition. Subsequently, either helium loss or CO_2 addition increases both $CO_2/^3He$ and $CO_2/^4He$ but does not affect the $^3He/^4He$ ratios. The second

process affects the majority of the springs (excluding Glenluce and Argyle) but none of the well gas samples (trajectory towards the CO_2 apex of the plot).

To evaluate this two-step process in the following discussion, we select two samples to use as initial end-members. Argyle spring is representative of the regional high-mantle end member, least affected by radiogenic ^4He addition (exhibiting the highest measured $^3He/^4He$ ratio 3.65 of R_c/R_A, $[^4He] = 8.8 \pm 0.3 \times 10^{-5}$ $cm^3(STP)/cm^3$). The highest He concentrations were measured in Glenluce sample ($^3He/^4He$ 1.57 R_c/R_A, $[^4He]=1.6 \pm 0.1 \times 10^{-4}$ $cm^3(STP)/cm^3$), which is the least affected by secondary He loss or CO_2 addition.

The $^3He/^4He$ ratio can be modified by dilution with non-CO_2 gas (usually methane) with a different He isotopic signature (Sherwood Lollar et al., 1994), radiogenic ^4He accumulation in situ (Newell et al., 2015; Liu et al., 2016) or He stripping from formation water during gas migration through lithological units enriched in ^4He (Sano et al., 1990; Sakamoto et al., 1992). The resulting $^3He/^4He$ ratio can then be overprinted by addition of CO_2 from a different source (O'Nions and Oxburgh, 1988) or phase fractionation during degassing (Matthews et al., 1987). If the well gases and CO_2 springs share a common source, then these processes can be accounted for and gas composition can be traced back to a single initial end-member.

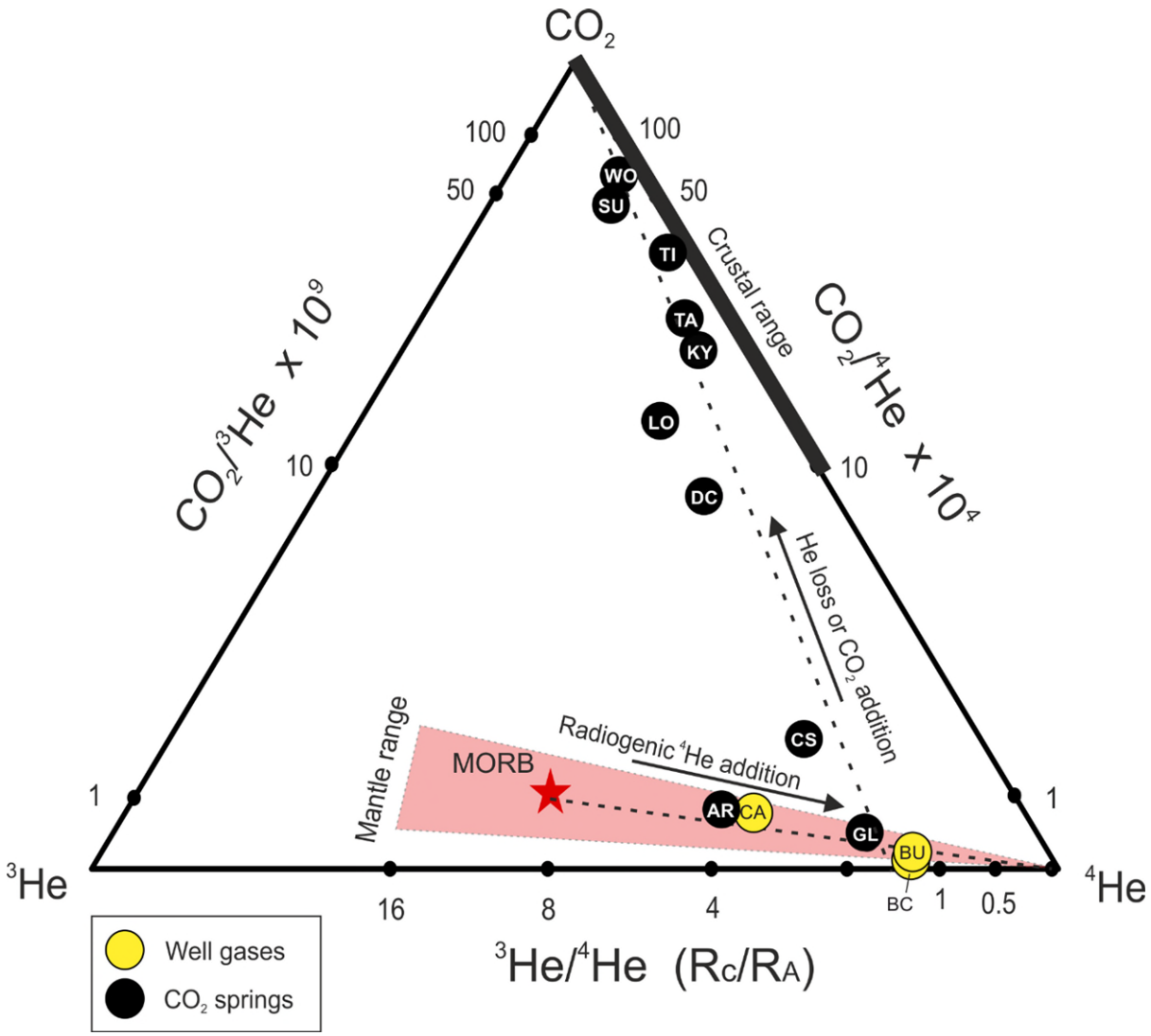

Figure 4. Ternary diagram (after Giggenbach et al., 1993) showing the relationship between the concentrations of CO_2, ^3He, ^4He expressed as their ratios. MORB value used for reference is 8 ±1 R_A (Marty and Jambon, 1987). The dashed lines show mixing between different components. The two clear trends are: 1) Radiogenic ^4He addition, which shifts gas composition to the right apex of the ternary plot, 2) CO_2 addition or He loss trend towards the top apex of the plot. Port Campbell well gases fall on the mixing line between MORB and crustal end-member. Spring samples fall on He loss/CO_2 addition trendline. Abbreviations of sample names are given in Table 1.

4.2 Radiogenic ^4He addition

^4He is produced by the alpha decay of uranium and thorium in the crust. These elements are primarily concentrated in accessory minerals such as zircon and apatite, which release helium at a constant rate above the blocking temperature of the mineral (Tolstikhin et al., 2017). Similarly, ^3He is produced by thermal neutron capture by ^6Li, which can be approximated based on Li content of the crust (Ballentine and Burnard, 2002). However, this contribution is minimal relative to the amount of

^{3}He released from mantle fluids and can be considered to be negligible in the context of in-situ crustal helium accumulation.

After production, radiogenic helium is either trapped in the pore spaces in-situ or mobilised by any migrating water or gas phase present in the subsurface and then transported elsewhere. If a natural gas trap exists in-situ, helium will preferentially accumulate in the gas phase due to its low solubility in water.

4.2.1. Radiogenic ^{4}He accumulation in-situ

The initial ^{3}He/^{4}He ratio of mantle-sourced gas can be reduced by direct accumulation of ^{4}He produced in the crust, or by mixing with ^{4}He-rich methane. The former would be applicable to CO_2 springs, the latter to well gases containing CO_2 and CH_4 mixtures. In both cases, the final ^{4}He concentrations are controlled by the rate of ^{4}He production in the crust. The contents of radiogenic ^{4}He accumulated in-situ in a natural gas trap can therefore be considered as a function of time since the initial emplacement of the gas in the trap, given a known crustal helium production rate (Liu et al., 2016). Under this assumption, we can estimate the residence time required for the observed ^{3}He/^{4}He ratios in both the well gases and the springs.

The ^{4}He production rate (Craig and Lupton, 1976) and ^{4}He concentration in the pore fluid increases at the rate of J_{He} (Torgersen, 1980):

$$^4P = 0.2355 \times 10^{-12} \times [\mathrm{U}] \times (1 + 0.123 \times [\mathrm{Th}]/[\mathrm{U}] - 4) \quad (1)$$

$$J_{He} = {}^4P \times \rho \times (1 - \phi)/\phi)) \quad (2)$$

Where:

$[\mathrm{U}]$, $[\mathrm{Th}]$ – concentrations in ppm

^4P – crustal ^{4}He production rate in cm^3 STP g^{-1} yr^{-1}

J_{He} – ^{4}He production rate cm^3 (STP) yr^{-1}

ρ – density of the crust in g/cm^3

ϕ – porosity of the rocks as a fraction

Assuming ^{4}He has been accumulating in mantle-sourced CO_2 with a known initial composition, the final ^{3}He/^{4}He ratio is expressed as a function of time (Newell et al., 2015):

$$^{3}He/\,^{4}He(t) = F \times\ ^{3}He_m/(J_{He} \times\ t\ +\ F \times\ ^{4}He_m) \quad (3)$$

Where:

F – gas volume fraction in the rock

He_m– helium concentration of the mantle end-member

t – time in years

The final result is independent of the timing of CO_2 emplacement as it records the total ^{4}He accumulated since the start of the gas trap filling, so in the case of CO_2/methane mixture, the recorded age will be that of the methane emplacement. Argyle spring concentrations are taken as representative of the initial mantle end-member, based on the highest measured $^{3}He/^{4}He$ ratio.

Assuming an average reservoir porosity of 25 % (Watson et al., 2003), average crustal ^{238}U and ^{232}Th concentrations of 2.8 and 10.7 ppm and assuming an average crustal density of 2.5 g/cm^3 (Rudnick and Fountain, 1995) the estimated age of filling of the of Boggy Creek field is 32 Ma (Fig 5). Assuming ± 5 % and ± 1 % uncertainty in porosity and ^{238}U and ^{232}Th concentrations respectively, the accumulation age could vary between 22 and 45 Ma (showed in shaded area in Fig 5). This calculated accumulation age range can be taken as a maximum, as the described method does not take into account the contribution of helium stripped from water during the two stages of gas migration in the reservoir and the initial ^{4}He contents of the gas phase acquired from the source rock. Methane in Port Campbell traps is associated with the last hydrocarbon generation stage that commenced during the mid-Paleogene (Duddy, 1997; Boreham et al., 2004), which closely matches the range of accumulation ages calculated. The $^{3}He/^{4}He$ ratios observed within the Boggy Creek and Buttress fields can plausibly be explained by an Argyle-type mantle end-member mixing with thermogenic methane containing radiogenic ^{4}He, confirming the binary mixing with methane trend depicted in Figure 4.

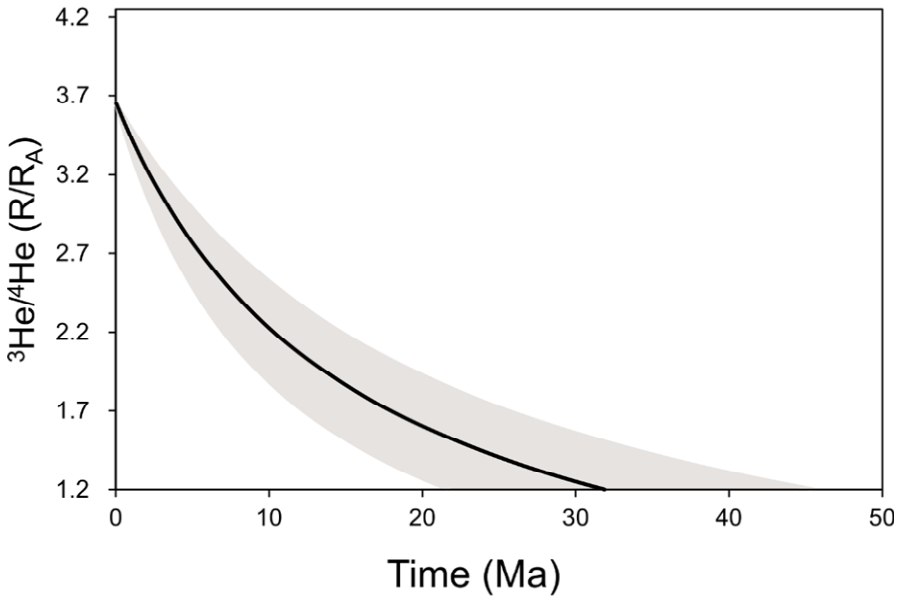

Figure 5. $^3He/^4He$ ratio vs time since gas emplacement calculated for the composition of the Boggy Creek-1 sample. To achieve the current $^3He/^4He$ ratio measured in Boggy Creek (1.21 R_A), Argyle-type CO_2 (3.65 R_A) would have to mix with methane that has been emplaced at 32 Ma. Shaded area shows uncertainty.

The same calculation can be applied to the CO_2 springs. ^{238}U-^{232}Th contents are assumed to be the same; the porosity of a fracture-dominated metasedimentary aquifer is estimated to be lower (10 ± 5 %). To reduce the initial $^3He/^4He$ ratios of 3.65 to the lowest measured value of 1.23 R_A, it would take 9 Ma years on average and between 4-15 Ma within the uncertainty of the parameters. To account for the range of observed $^3He/^4He$ ratios, this scenario requires emplacement of separate gas pockets for each individual spring at different times between 9 Ma and present and retention within the crust before the onset of the recent migration to the surface.

Multiple gas injection events could be associated with discrete episodes of seismic or volcanic activity, although the latter is unlikely because the volcanic cones are far fewer than the individual mineral springs (>100) (Shugg, 2009), and given the predominately monogenetic eruptive character of the NVP extrusives (Boyce, 2013) volcanic activity is unlikely to produce so many different gas pulses. Irrespective of the gas emplacement mechanism, the heavily folded and fractured Ordovician metasedimentary sequence is unlikely to act as an effective gas trap for millions of years. In-situ ^4He accumulation in CO_2 springs is therefore an unlikely process to account for the observed variation in $^3He/^4He$ ratios.

4.2.2. Radiogenic ^4He stripping from enriched pore-water

An alternative model to in-situ generation is modification of magmatic $^3He/^4He$ ratios by dilution of mantle He during lateral movement of the CO_2 by radiogenic ^4He stripping from formation

water. This is a different process to interaction with ASW, which has already been accounted for using He/Ne ratios to correct $^{3}He/^{4}He$ values for contribution of the atmospheric component sourced from the formation water (Fig. 2). Instead, the stripping model considers radiogenic helium accumulated and contained in the pore water of U/Th-enriched rocks. In this case the process is still governed by the helium production rate in the crust (similar to the in-situ ^{4}He accumulation discussed above), but the controlling factor is distance rather than time.

Assuming that mantle fluids are supplied through a single conduit at a constant rate under steady-state homogenous and isotropic conditions under an equal hydrostatic pressure, the variation in $^{3}He/^{4}He$ values can be accounted for by a hydrodynamic dispersion model (Sano et al., 1990). $^{3}He/^{4}He$ is calculated as a function of the radial distance to the conduit (r) following the approach detailed in Sano et al. (1990) of deriving the location-specific helium dispersion constant (α) by fitting a least squares function to the measured $^{3}He/^{4}He$ and radial distance data points.

$$^{3}He/\,^{4}He(r) = (\,^{3}Pr^{2} + \alpha\,^{3}He_{m})\,)/(\,^{4}Pr^{2} + \alpha\,^{4}He_{m})) \quad (4)$$

Where:

r – radial distance from the main gas conduit

α – helium dispersion constant, dependent on the pore network geometry

P – crustal helium production rate in atoms/cm^{3}s, calculated under the same crustal density and U, Th content assumptions as in the ^{4}He accumulation model.

The Argyle spring (highest measured $^{3}He/^{4}He$ ratio of 3.65 R_A) is taken to be the closest to the main conduit of mantle degassing in the CVH. Figure 6a shows the relationship between the $^{3}He/^{4}He$ ratios and the radial distance of sample location to the Argyle spring. Kyneton spring is excluded from this because of its contamination with an atmospheric component. Samples with higher $^{3}He/^{4}He$ ratios are located geographically closer to each other and the Argyle spring (Fig. 6b). Hence, we propose that mantle CO_2 is being progressively diluted with a crustal component with increasing distance from the inferred conduit.

The majority of the CO_2 migration prior to the degassing point occurs within the subsurface, through ^{4}He-enriched basement rocks. The interaction with shallow ASW water occurs only at the final stages of migration during the ascent to the surface, which explains the relatively high $^{4}He/^{20}Ne$ ratios and low atmospheric ^{20}Ne content in the majority of the samples. Similar decreases in $^{3}He/^{4}He$ ratios with increasing distance from a central volcanic cone has been observed in various active

411 volcanoes (Marty and Jambon, 1987; Williams et al., 1987; Sano et al., 1990; Sakamoto et al., 1992).
412 The $^{3}He/^{4}He$ distribution pattern is location-specific and controlled by the differences in the
413 topographic profile and the tortuosity of the fracture network, represented as constant α in
414 Equation 4.

415 The overall average rate of $^{3}He/^{4}He$ decrease in 4 volcanic locations reviewed by Sakamoto et
416 al. (1992) varied between 0.3 to 0.5 R_A/km. The average rate of $^{3}He/^{4}He$ decrease in CVH is 0.1
417 R_A/km, potentially reflecting fluid migration via more efficient fracture networks and conduits in a
418 faulted sequence relative to the previously investigated volcanic and volcanoclastic sequences.
419 Fractured aquifers have lower tortuosity relative to porous ones, which results in shorter effective
420 travel distance for the same total flow path distance (Clennell, 1997) and therefore lower rate of
421 radiogenic noble gas stripping per distance travelled.

422 Springs with the highest $^{3}He/^{4}He$ ratios are clustered near the N-S trending Muckleford Fault
423 and a smaller parallel fault striking along Lake Daylesford (Fig 6b). The spatial distribution of $^{3}He/^{4}He$
424 ratios controlled by helium dispersion along the flow pathways from the main conduit suggests that
425 one of these basement lineaments could be acting as a conduit through which mantle CO_2 is being
426 charged from depth. Previous studies have shown that clusters of NVP volcanic vents are commonly
427 aligned parallel to nearby basement faults throughout the province (van Otterloo et al., 2013; Cas et
428 al., 2017). Mantle xenoliths were found in the vicinity of the faults, suggesting fast mantle upwelling
429 rates through the lithosphere were prevalent during periods of magmatic activity (van Otterloo et
430 al., 2014). While further work is required to provide geomechanical and structural geological
431 evidence for current fluid migration along the fault zones in the CVH, these structures can
432 potentially play an important role in the currently active mantle-CO_2 ascent to the surface.

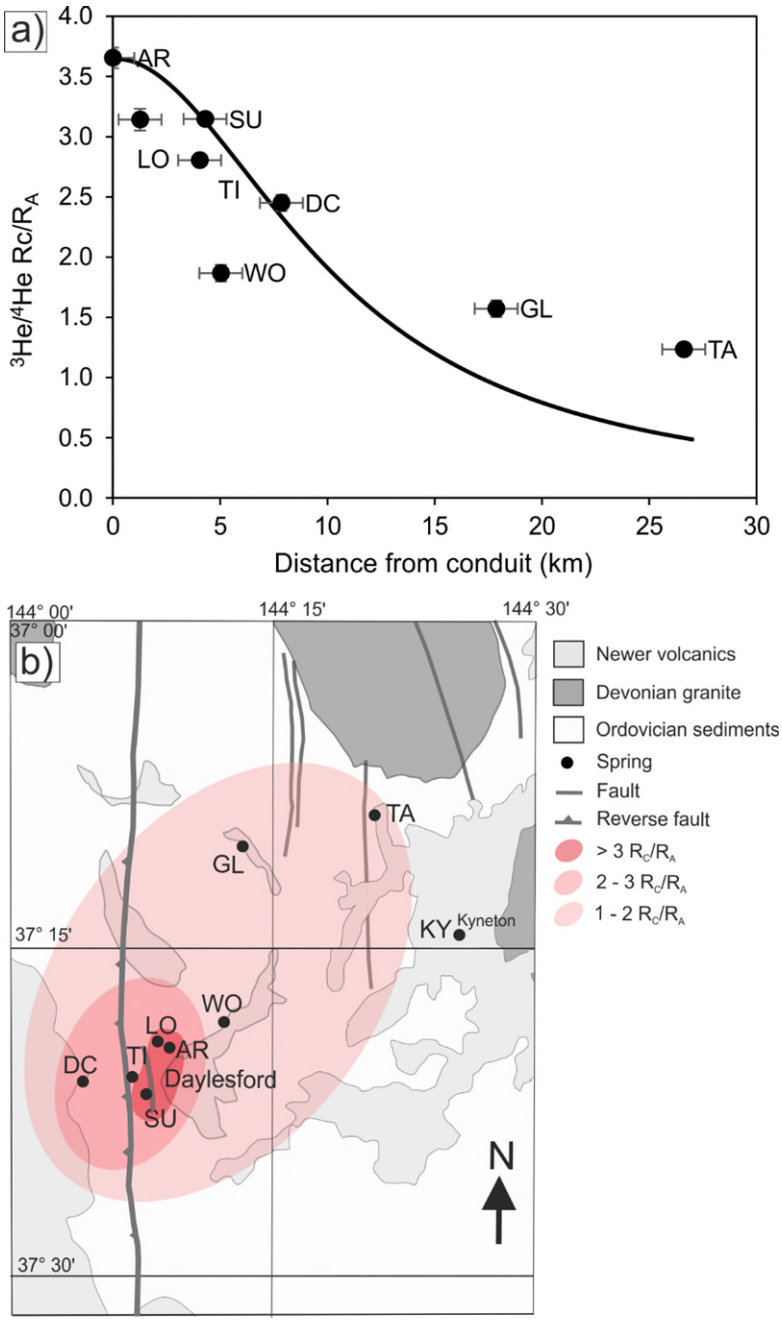

433

434 **Figure 6 a). Plot of ^{3}He/^{4}He Rc/R$_A$ values relative to the distance from the main conduit (measured on**
435 **Google Earth) taking the highest ^{3}He/^{4}He ratio of Argyle spring as a starting value. The solid line is ^{3}He/^{4}He**
436 **dispersion with distance model calculated based on (Sano et al., 1990). b). Geographical distribution of CO_2**
437 **springs. Springs with the highest ^{3}He/^{4}He ratios are clustered close to N-S trending basement-scale**
438 **Muckelford thrust fault and parallel smaller fault near Lake Dayleford. Shaded areas show ^{3}He/^{4}He ratio**
439 **ranges which decrease with increasing distance from the Argyle spring. Kyneton spring is excluded due to**
440 **atmospheric contamination. Abbreviations of sample names are given in Table 1**

441

4.3. Evaluating models to account for $CO_2/^3He$ variation

The combination of CO_2 and helium is often used to identify the presence of mantle volatiles. This is because $CO_2/^3He$ ratios have been well constrained for mantle-derived melts, fluids and volatiles, with an average MORB value accepted as $1.5 \pm 0.5 \times 10^9$ (Sano and Marty, 1995; Marty and Tolstikhin, 1998). ^3He is not produced in significant amounts in the crust, so low ^3He ratios and associated $CO_2/^3He$ ratios between $10^{10} – 10^{15}$ are typically associated with a crustal CO_2 source (O'Nions and Oxburgh, 1988). A trend in increasing $CO_2/^3He$ ratios is therefore often associated with admixture of crustal CO_2 (e.g. Crossey et al., 2009; Newell et al., 2015; Ruzié et al., 2013). The $CO_2/^3He$ ratios observed in ten CO_2 samples from the Victorian mineral springs vary over two orders of magnitude (2.8×10^9 to 6.5×10^{11}), encompassing the range typical of mantle and crust end-members.

Crustal end-members can have a wide range of $CO_2/^3He$ ratios but a narrow range of $^3He/^4He$ ratios (0.01 – 0.07) (Ozima and Podosek, 2002). Figure 7 shows $CO_2/^3He$ values plotted against $^3He/^4He$ R_c/R_A ratios with binary mixing curves representing mantle (8 R_A) source and various crustal components. Significantly, samples with high $CO_2/^3He$ ratios do not necessarily show lower $^3He/^4He$ ratios, as would be expected in the case of mixing with ^3He-poor crustal CO_2 source and trend perpendicular to the calculated mixing lines. To explain the range of measured $CO_2/^3He$ ratios, variable amounts of mixing with a wide range of different crustal reservoirs ($CO_2/^3He – 10^{10}$ - 10^{14}) would need to be invoked, which is unlikely in the setting where bedrock geology is uniform across the area.

Crustal CO_2 addition can be further assessed by combining He data with $\delta^{13}C(CO_2)$ values (Sano and Marty, 1995). The range of $\delta^{13}C(CO_2)$ values measured in the springs (-9.4 to -6‰) are outside the typical mantle (-7 to -4‰) range (Wycherley et al., 1999). However, increasing $CO_2/^3He$ ratios do not consistently correlate with $\delta^{13}C(CO_2)$ change towards carbonate or organic end-members (Fig. 8). Instead, a vertical trend exists, which would require mixing with an end-member with constant proportions of both organic and carbonate-sourced CO_2. To explain the highest observed $CO_2/^3He$ ratios, 99 % of non-mantle (crustal/organic mixture) CO_2 addition is required. Such significant amounts of crustal CO_2 sourced by dissolution of bedrock minerals would liberate cations contained in the dissolving minerals and increase the TDS values of the water. Figure 9 shows that there is no clear positive correlation between the $CO_2/^3He$ ratios in the volatiles and TDS values in their associated waters.

Previous geochemical modelling work showed that CO_2 does not cause significant amounts of bedrock mineral dissolution in the Ordovician aquifer (Karolytė et al., 2017) and there is no geological evidence for addition of large amounts of crustal CO_2 from other sources (e.g. carbonate metamorphism). The possibility of significant amounts of organic CO_2 addition is also ruled out, because the observed trend on Figure 8 cannot be explained by addition of organic CO_2 in the absence of the crustal component. Based on the combined evidence from $\delta^{13}C(CO_2)$-He, CO_2 abundance and TDS contents of the mineral waters, we conclude that there is no significant crustal CO_2 addition to the mantle volatiles sampled at the CVH and Clifton Springs.

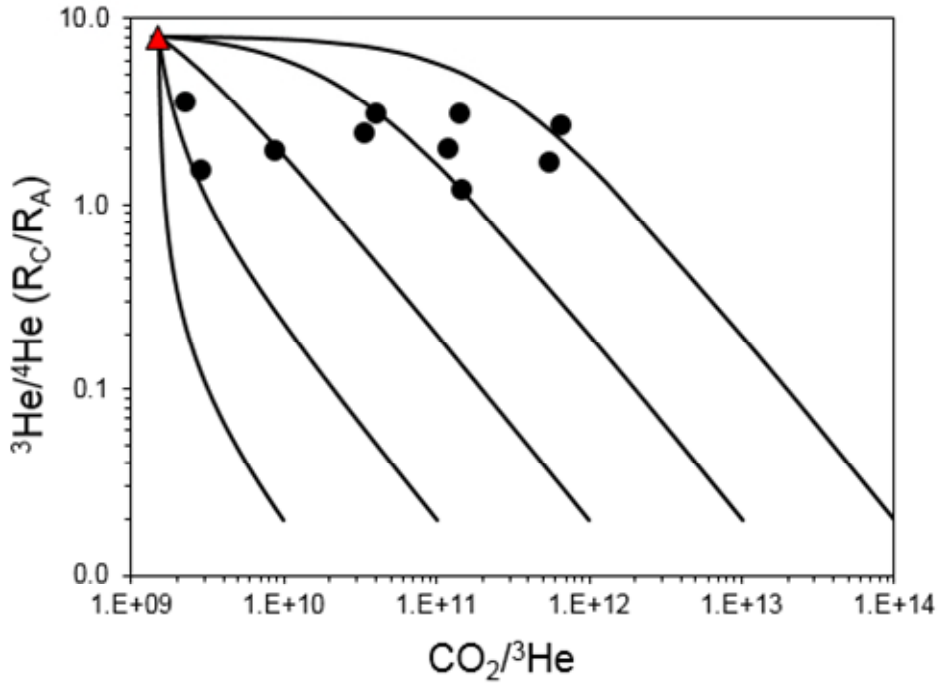

Figure 7. Binary mixing plot between MORB (red triangle) ($^3He/^4He$ 8 R_A, $CO_2/^3He$ 1.5 x 10^9) and various crustal end-members ($CO_2/^3He$ 10^{10}-10^{14}). The springs form a near-horizontal trendline and do not follow any of the mixing lines, suggesting that mixing does not control the variation in $CO_2/^3He$ values. All error bars are smaller than the printed symbols.

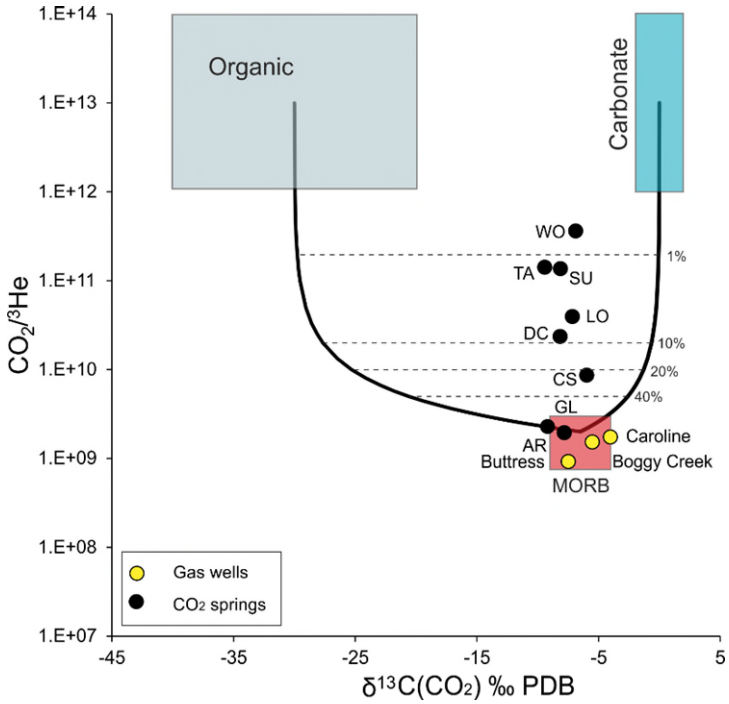

Figure 8. $CO_2/^3He$ ratios vs $\delta^{13}C$ values for gas samples in relation to mixing between the mantle, carbonate and organic CO_2 end-members based on Sano and Marty, 1995. Caroline, Boggy Creek and Buttress well gases fall within the mantle range. Spring samples do not show a coherent trend towards either an organic or carbonate CO_2 end member. The observed trend would require > 99% contribution of a component with constant proportions of both organic and carbonate-sourced CO_2; however, this is not supported by other data (discussed in text). Abbreviations of sample names are given in Table 1.

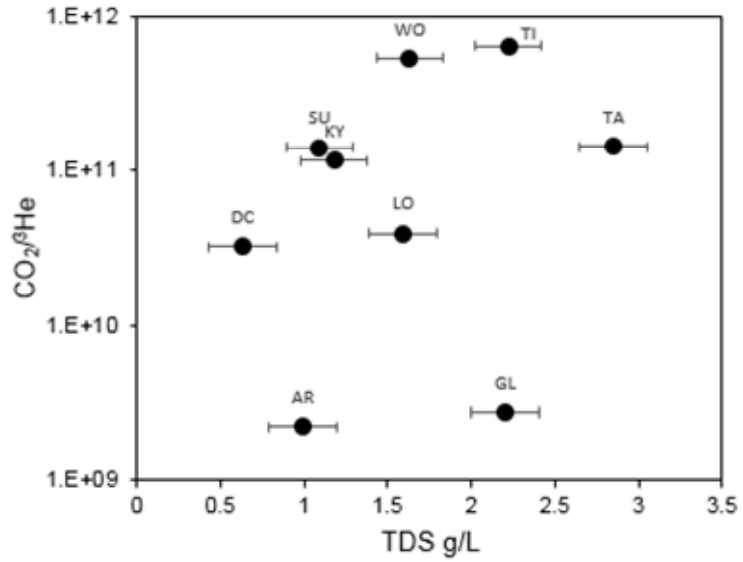

Figure 9. $CO_2/^3He$ vs TDS measured in borehole water sampled via hand pumps. $CO_2/^3He$ values are not correlated with TDS. A positive correlation would be expected if crustal CO_2 was added as a result of bedrock mineral dissolution.

Alternatively to mixing with different CO_2 sources, the variability of $\delta^{13}C(CO_2)$ values (-9.4 to -6‰) can be explained by degassing under a range of different pH and temperature conditions. Equilibrium fractionation between $\delta^{13}C(CO_2)$ in aqueous and gaseous phases is controlled by the temperature and the relative amounts of HCO_3^- and H_2CO_3, which are pH-dependent. If H_2CO_3 is the dominant DIC species, degassing CO_2 is slightly enriched in ^{13}C. Conversely, when HCO_3^- dominates the system, degassing CO_2 is relatively depleted in ^{13}C (Deines et al., 1974). The pH values measured in mineral water bores range from 5.5 to 6.1 and temperatures are 15 – 21 °C. In this particular range of conditions, the ratio of HCO_3^- to H_2CO_3 in DIC varies significantly. The resulting calculated equilibrium enrichment factors between DIC and gaseous CO_2 range from -3.4 to -0.43‰. Degassing under different DIC speciation conditions therefore can fully account for the observed 3.4‰ variability in $\delta^{13}C(CO_2)$ values of the spring gases.

4.4 Noble gas abundance modification by near-surface degassing

The variation observed in ^3He concentrations in the mineral spring samples is also replicated in ^4He and other noble gases. Importantly, the range in which concentrations vary decreases with element mass (Fig. 10). This suggests that the large differences in elemental abundance between the spring samples could be caused by a physical fractionation, post-dating the mixing of mantle and ASW sources. CO_2 springs are a dynamic two-phase system where equilibrium partitioning between water and gas during mineral water ascent to the surface is likely to occur.

515 Noble gas solubility in water increases with element mass. During equilibration in a two-phase
516 water and gas system, noble gases are partitioned between gas and water according to their
517 solubility coefficient, as defined by Henry's Law (Ballentine et al., 2002):

518 $$C_{ig} = K_i \times C_{iw} \quad (5)$$

519 Where C is concentration, subscripts g and w denote gas and water phases and K_i is Henry's
520 constant for noble gas *i*. K_i is temperature, pressure and salinity dependent (Kipfer et al., 2002). For
521 the purpose of investigating a shallow degassing process, we assume equilibration with fresh water
522 at atmospheric pressure and 20 °C temperature. Henry's constants and activity coefficients for water
523 conditions were calculated from empirical equations from Crovetto et al. (1982) for Ne, Ar, Kr and Xe
524 and Smith (1985) for He, following the methodology in Ballentine and Burnard (2002).

525 In a closed system, the total noble gas contents are conserved but redistributed between the
526 two phases according to the relative gas/water volume ratios. In the situation where the initial
527 concentration in the gas phase is known (C_{ig}^0), the associated equilibrium concentration in water
528 (C_{iw}^0) can be calculated from Equation 5. Redistribution of the noble gas contents between the two
529 phases can then be expressed as a function of volume, where $\frac{V_g}{V_t}$ is the fraction of the total volume
530 occupied by gas and C_{ig}^f is the final concentration is the gas phase:

531 $$C_{ig}^f = C_{ig}^0 \times \frac{V_g}{V_t} + C_{iw}^0 \times (1 - \frac{V_g}{V_t}) \quad (6)$$

532 The final noble gas concentrations measured in CO_2 degassing at the surface are a result of the
533 initial dissolution in water and subsequent degassing, which can occur in two or more steps under
534 different water/gas ratios. However, the final result is independent of these variations as long as the
535 system remains closed. In reality, solubility constant K_i will differ slightly during dissolution and
536 degassing steps depending on depth and temperature conditions, but the overall difference will be
537 far smaller than that caused by the difference in gas/water volume ratios.

538 A scenario where $\frac{V_g}{V_t} = 1$ describes simple equilibrium partitioning at given pressure and
539 temperature, in this case under atmospheric pressure at the surface, where there are no constraints
540 other than atmospheric pressure to the volume of the gas phase. In this case $C_{ig}^f = C_{ig}^0$ and water
541 noble gas contents are in accordance with atmospheric equilibrium. In the opposite case, when gas
542 volume fraction ratio is becoming infinitesimally small ($\frac{V_g}{V_t} \to 0$), noble gas contents are dissolved in
543 water and $C_{ig}^f \to C_{iw}^0$. The $\frac{V_g}{Vt} \to 0$ scenario describes a situation where constraints in space limit the

volume expansion and result in overpressure. Because volume ratios are expressed as a fraction of the total volume, the possible values range from 0 to 1.

The wide range of noble gas concentrations in the CO_2 springs allows a test of whether variations in $\frac{V_g}{V_t}$ ratios correlate with measured noble gas contents consistently across different element pairs. The highest helium concentrations were measured in Glenluce spring, which is taken to be representative of the least fractionated gas phase. We make an assumption that Glenluce degassed under $\frac{V_g}{V_t} = 1$ conditions with no external gas stripping mechanism based on field observations of intermittent bubble formation and an overall low CO_2 flux. Under these assumptions C_{ig}^f can be calculated for different $\frac{V_g}{V_t}$ ratios. This approach does not require separate calculation of noble gases degassing from ASW, as the final noble gas concentrations measured from each spring are a sum of the total noble gas contents derived from the both water and the original mantle sources.

Figure 10 shows the distribution of noble gas concentrations in the studied springs. The range in observed gas concentrations decreases with element mass. The solid black line shows concentrations of $\frac{V_g}{V_t} = 1$ where no fractionation between elements occurs and the final concentrations are the same. The dashed line shows $\frac{V_g}{V_t} = 0.01$ scenario where fractionation is close to the maximum possible in a closed system and $C_{ig}^f \rightarrow C_{iw}^0$. All data points plot within the bounds of these two end-member scenarios and can therefore be interpreted as fractionated within a closed system. The progressive loss of noble gas concentrations correlates across all noble gas elemental pairs.

Figure 11 shows ^{3}He concentrations relative to ^{4}He, ^{20}Ne, ^{40}Ar, ^{84}Kr and ^{132}Xe. Solid blue lines show calculated fractionation trends from the initial composition of Glenluce, with black tick marks showing the $\frac{V_g}{V_t}$ ratio. The noble gas concentrations follow a negative trend in all elemental pairs with $\frac{V_g}{V_t}$ ranging from 0.3 (Clifton Springs) to 0.01 (Taradale and Sutton). Deviation from a closed system scenario occurs if the system is partially open to gas or water loss and input. Gas can be added by mixing with air, both gas and water can be added by admixture of ASW and finally gas can be removed from the system prior to the point of sample collection. If gas is lost prior to sampling, equation 6 no longer holds true and the final gas concentrations are not limited to those of the initial water ($\frac{V_g}{V_t} \rightarrow 0$, $C_{ig}^f \rightarrow C_{iw}^0$ scenario). Alternatively, the initial gas concentration C_{ig}^0 could be modified by mixing with ASW or air.

574 ^{3}He and ^{4}He values in Tipperary and Woolnoughs springs are lower than predicted by the
575 closed system model, which can be explained by mixing with both ASW and water (Fig. 11). This is
576 obvious in different element pair plots (Figs. 11 b,c,d,e) and less apparent in ^{3}He vs ^{4}He (Fig. 11a)
577 because air and ASW have similar $^{3}He/^{4}He$ ratios. Figure 11b also clearly shows that solubility
578 fractionation in Kyneton spring has been overprinted by admixture of air, most likely during sample
579 collection and clearly identified in the $^{4}He/^{20}Ne$ ratios, as previously mentioned. Clifton Springs,
580 Deep Creek, Locarno and Taradale samples plot between solubility fractionation and mixing with
581 ASW lines in Figure 11 c,d,e illustrating the additions of a small component derived from ASW, the
582 influence of which is more evident in the heavier atmospheric noble gases.

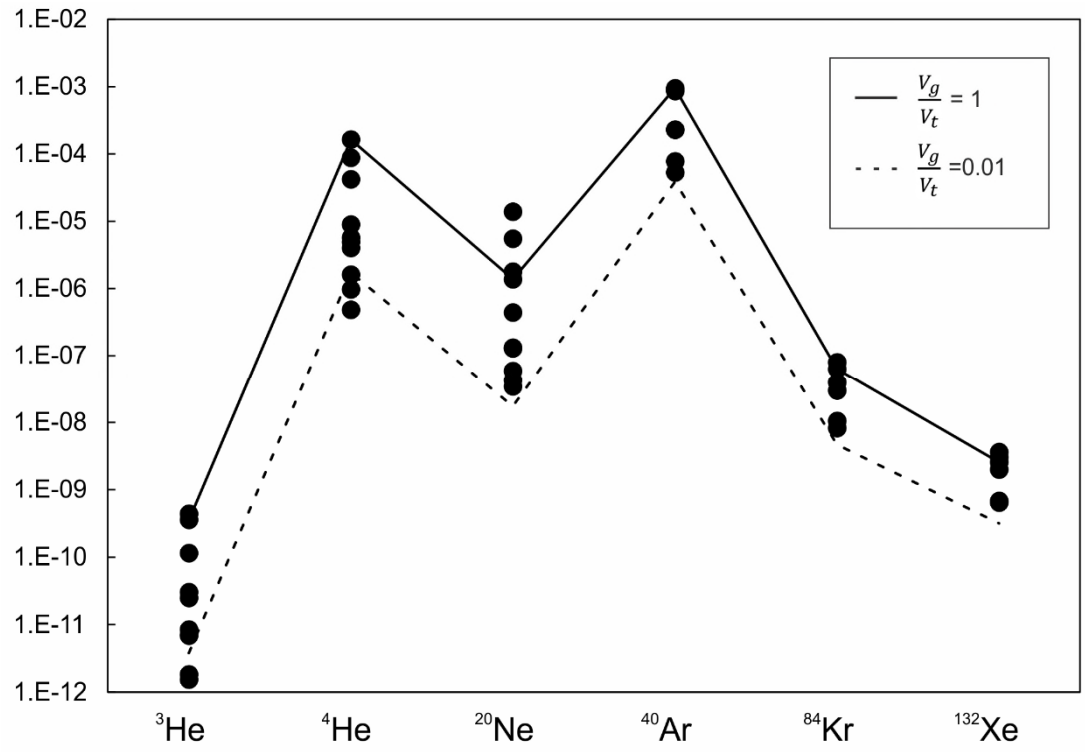

583

584 **Figure 10. Noble gas concentrations of CO_2 spring samples in cm^3 (STP)/cm^3. The variation in concentrations**
585 **decreases with relative noble gas mass. This is explained by partitioning between water and gas phases**
586 **during degassing, assuming a closed system. Black solid and dashed lines show expected gas concentrations**
587 **for final V_g/V_w ratios of 1 and 0.01, respectively. The data are in good agreement with the model indicating a**
588 **closed system, with exceptions of depletion in He and enrichment in Ne in samples that have equilibrated**
589 **with a mixture of ASW and air (discussed in text). The extent of fractionation for different noble gases**
590 **decreases with increasing mass and is directly dependent on their relative solubilities in water.**
591 **Abbreviations of sample names are given in Table 1.**

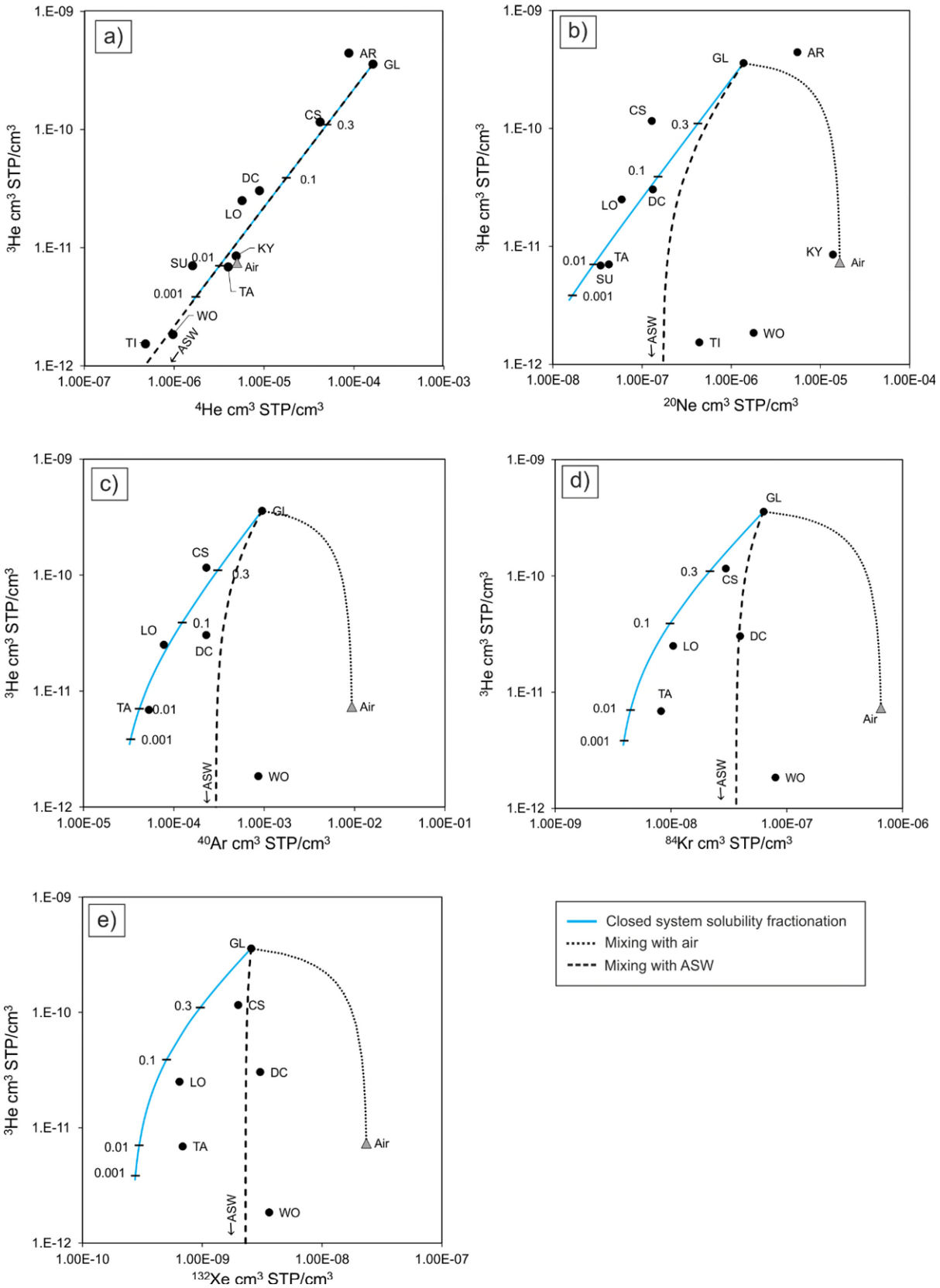

592

593 **Figure 11. ^{3}He concentrations relative to ^{4}He (a), ^{20}Ne (b), ^{40}Ar (c), ^{84}Kr (d) and ^{132}Xe (e) in cm^{3}(STP)/cm^{3}. Solid**
594 **black lines show calculated concentrations assuming degassing from the initial Glenluce composition, with**
595 **decreasing V_g/V_t ratio from 1 to 0.001, marked by black tick marks. Dashed lines show mixing with ASW at**

20 °C; dotted line shows mixing with air. All samples can be explained by fractionation during degassing at V_g/V_t ranging from 1 to 0.01 with some deviation from the calculated trendline due to mixing with ASW and/or air. a) All samples fall within the calculated line except for TI and WO springs. b) shows that this is because TI and WO have a contribution between ASW and air components, plotting between these end-members. This is consistently replicated for Woolnoughs spring in c) d) and e). Ar, Kr and Xe concentrations of CS, DC, LO and TA springs are within the limits of mixing with ASW and calculated degassing fractionation line. Abbreviations of sample names are given in Table 1.

The conceptual model of CO_2 migration to the surface is summarised in Figure 12. The initial mixing between mantle and ASW noble gas components occurs when mantle CO_2 migrates and dissolves in groundwater. The mineral water with dissolved noble gas contents ascends to the surface via individual restricted fracture corridors and manifests at the surface as separate geographically dispersed springs. The nucleation of the gas phase in water occurs when partial pressures of dissolved gases exceed the hydrostatic pressure. Partial pressures of noble gases are too low to trigger the degassing at depth, so the process is controlled by the CO_2 saturation level of the water. Once the dominating gas phase (CO_2) is oversaturated and begins degassing, the other dissolved gas species will partition between the two phases based on gas/water volumetric ratio.

After equilibrium separation water and CO_2 migrate to the surface as a two-phase flow and do not re-equilibrate again. This implies that in instances where degassing occurs at depth, sampled gases are expected to contain lower concentrations of noble gases because of the limiting effect of gas volume being restricted to that of CO_2. In contrast, mineral waters with lower CO_2 partial pressures nucleate into the gas phase at surface equilibrium conditions and therefore contain higher overall noble gas contents. This finding suggests that noble gas tracing of shallow leakage is more sensitive and the original composition is better preserved where overall CO_2 partial pressures are lower and degassing occurs at or very near to the surface. Noble gases are therefore particularly sensitive tracers to small scale gas migration and should be considered for surface monitoring of any industrial site where fugitive gas emission is a possibility.

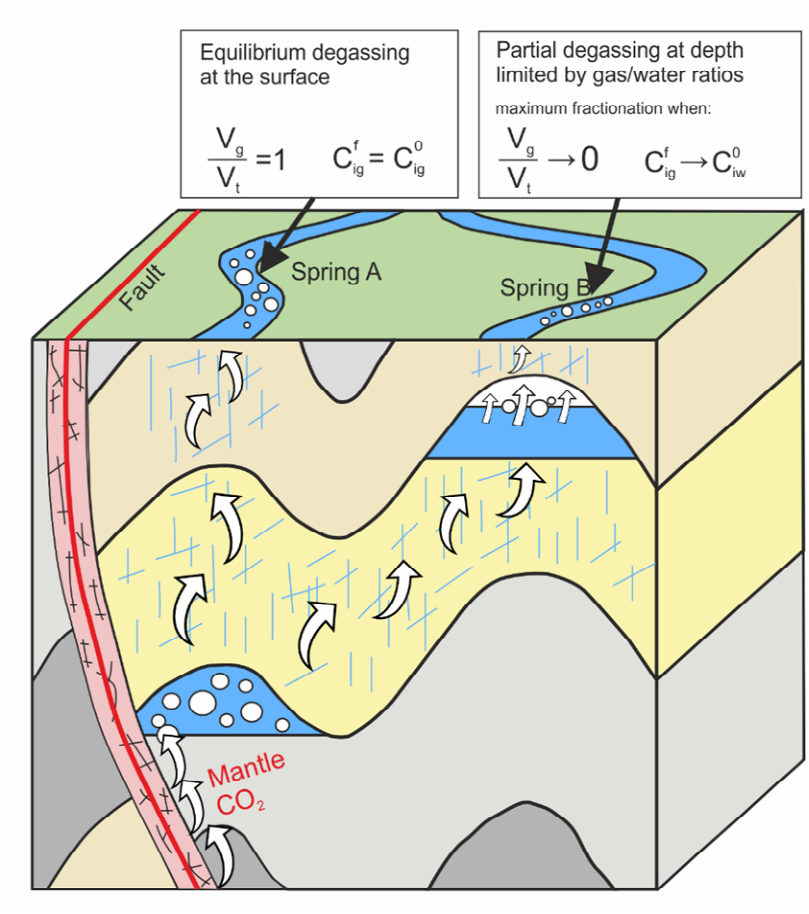

622

623 **Figure 12. Schematic cartoon of CO_2 and mineral water migration. Mantle CO_2 ascends through a fault zone**
624 **and dissolves in groundwater. Water charged with CO_2 migrates through a fractured aquifer to the surface.**
625 **In spring A, with a low gas flux, gas/water separation occurs at the surface under equilibrium conditions and**
626 **the final degassed gas phase retains its original concentrations. In the case of spring B, with a higher gas flux,**
627 **gas/water separation occurs at depth when CO_2 becomes oversaturated in water. Noble gases partition**
628 **between water and gas phases under the same equilibrium conditions, but the partitioning is limited by the**
629 **gas volume.**

5. Conclusions

$^3He/^4He$ and $CO_2/^3He$ ratios in well gas and CO_2 spring samples in the Otway Basin and the Central Victorian Highlands show unambiguous evidence for a predominantly mantle origin for the CO_2 stored in the gas fields and actively migrating to the surface at the springs. The main processes modifying noble gas geochemical signatures are crustal ^4He addition and noble gas fractionation between the water and gas phases during degassing. $^3He/^4He$ ratios in well gases vary due to mixing with methane, which has crustal helium contents directly dependent on gas residence time in the reservoir.

The $^3He/^4He$ ratio variation in CO_2 springs is controlled by hydrodynamic dispersion and is directly dependent on the radial distance to the gas supply conduit. The observed decline in $^3He/^4He$ ratios with distance suggests that CO_2 is supplied from a single conduit in the area around Argyle spring. $^3He/^4He$ ratios are the highest in samples clustered near the Muckleford Fault and smaller parallel faults in its vicinity, suggesting that one of these basement lineaments could be acting as a pathway for mantle CO_2 to reach the shallow subsurface.

The variability of noble gas abundance patterns observed in the CO_2 springs can be explained by closed system solubility fractionation during degassing. The gas to water ratio at the time of phase separation controls the distribution of noble gases between the water and gas phases. The original noble gas composition of CO_2 springs is uniform and only altered by near-surface degassing during the final stages of CO_2 ascent to the surface, dependent on CO_2 flux; the $\delta^{13}C(CO_2)$ values are controlled by degassing at pH range of 5.8 - 6.3. Original noble gas signatures are better preserved in samples where overall CO_2 partial pressures are lower and degassing occurs at or very near the surface.

Taking these processes into account, noble gas compositions observed in well gases in Port Campbell, Mount Gambier, as well as CO_2 springs in CVH and Clifton Springs are traced back to a single end member of $^3He/^4He$ of 3.07 - 3.65 R_A, proving a common source. This implies a uniform regional gas composition in the Otway basin and CVH.

Importantly, we present evidence that ^3He loss resulting in high $CO_2/^3He$ ratios, commonly associated with crustal CO_2 addition, can be explained without the need to invoke mixing with crustal CO_2, which is especially important in the absence of a clear mixing trend in $\delta^{13}(CO_2)$values. Hence, $CO_2/^3He$ values should be compared to the concentrations of other noble gases and used with caution when assessing the origin of CO_2 degassing at surface springs.

The techniques outlined in this paper can be used to identify the origin of CO_2 seeps at the surface and their connectivity to reservoir gases. Hence, they can be applied to CO_2 sequestration or other industrial fugitive gas monitoring settings, such as surrounding shale gas operations. Helium-CO_2 abundance relationship can be used to determine the gas connectivity as long as the industrial gas has a different initial He isotope ratio to the ASW end-member. The genetic link between separate CO_2 seeps can be tested by applying solubility fractionation modelling to account for changes in noble gas concentrations caused by near-surface degassing.

Noble gas signatures have been observed to be better preserved in cases where CO_2 saturation levels in water are low and degassing occurs near or at the surface. This means that noble gases are therefore particularly sensitive tracers to small-scale gas migration and should be considered for surface monitoring of any industrial site where emission of fugitive gas is possible.

Acknowledgments

This work was supported by an EPSRC PhD studentship in partnership with CO2CRC and Badley Geoscience Ltd. G. Johnson and S. Gilfillan were partially supported by both UKCCSRC and Scottish Carbon Capture and Storage (SCCS), S. Serno was funded by the UK Carbon Capture and Storage Research Centre (UKCCSRC) Call 2 grant. S. Flude was supported by by EPSRC grant #EP/K036033/1. We thank the field operators – BOC, Air Liquide and CO2CRC for permission to sample the gas reservoirs. Craig Vivian and Peter Dumsey are thanked for support while sampling in the field. We thank Terry Donnelly and Marta Zurakowska at SUERC for assistance in obtaining stable isotope and noble gas measurements of gas samples. Ian Cartwright is thanked for providing background data on the Daylesford springs.

References

Aeschbach-Hertig W., El-Gamal H., Wieser M. and Palcsu L. (2008) Modeling excess air and degassing in groundwater by equilibrium partitioning with a gas phase. *Water Resour. Res.* **44**, 1–12.

Aka F. T., Kusakabe M., Nagao K. and Tanyileke G. (2001) Noble gas isotopic compositions and water/gas chemistry of soda springs from the islands of Bioko, São Tomé and Annobon, along with Cameroon Volcanic Line, West Africa. *Appl. Geochemistry* **16**, 323–338.

Akbari V. (1992) *Boggy Creek No.1 Well Completion Report*., Available at: http://geoscience-web.s3-website-ap-southeast-2.amazonaws.com/well/boggycreek1.htm.

Baines S. J. and Worden R. H. (2004) The long term fate of CO2 in the subsurface: natural analogues for CO2 storage. In *Geological Storage of Carbon Dioxide* (ed. R. H. Baines, S.J., Worden). Geological Society, London. pp. 59–85.

Ballentine C. J. (1997) Resolving the mantle He/Ne and crustal 21Ne/22Ne in well gases. *Earth Planet. Sci. Lett.* **152**, 233–249.

Ballentine C. J., Burgess R. and Marty B. (2002) Tracing Fluid Origin, Transport and Interaction in the Crust. *Rev. Mineral. Geochemistry* **47**, 539–614.

Ballentine C. J. and O'Nions R. K. (1994) The use of natural He, Ne and Ar isotopes to study hydrocarbon-related fluid provenance, migration and mass balance in sedimentary basins. *Geol. Soc. London, Spec. Publ.* **78**, 347–361.

Ballentine C. J., O'Nions R. K. and Coleman M. L. (1996) A Magnus opus: Helium, neon, and argon isotopes in a North Sea oilfield. *Geochim. Cosmochim. Acta* **60**, 831–848.

Barry P. H., Lawson M., Meurer W. P., Warr O., Mabry J. C., Byrne D. J. and Ballentine C. J. (2016) Noble gases solubility models of hydrocarbon charge mechanism in the Sleipner Vest gas field. *Geochim. Cosmochim. Acta* **194**, 291–309.

Bernecker T. and Moore D. H. H. (2003) Linking basement and basin fill: implications for hydrocarbon prospectivity in the Otway Basin Region. *APPEA J.* **43**, 39–58.

Boreham C. J., Hope J. M., Jackson P., Davenport R., Earl K. L., Edwards D. S., Logan G. A. and Krassay A. A. (2004) Gas – oil – source correlations in the Otway Basin, southern Australia. In Petroleum Exploration Society of Australia (PESA). pp. 19–22.

710 Boreham C., Underschultz J., Stalker L., Kirste D., Freifeld B., Jenkins C. and Ennis-King J. (2011)
711 Monitoring of CO2 storage in a depleted natural gas reservoir: Gas geochemistry from the
712 CO2CRC Otway Project, Australia. *Int. J. Greenh. Gas Control* **5**, 1039–1054.

713 Bosch A. and Mazor E. (1988) Natural gas association with water and oil as depicted by atmospheric
714 noble gases: case studies from the southeastern Mediterranean Coastal Plain. *Earth Planet. Sci.*
715 *Lett.* **87**, 338–346.

716 Boult P. J., Johns D. R. and Lang S. C. (2004) Subsurface plumbing of the Crayfish Group in the Penola
717 Trough: Otway Basin. In *Eastern Australasian Basins Symposium II* Petroleum Exploration
718 Society of Australia (PESA). pp. 483–498.

719 Boyce J. (2013) The Newer Volcanics Province of southeastern Australia: a new classification scheme
720 and distribution map for eruption centres. *Aust. J. Earth Sci.* **60**, 449–462.

721 Caffee M. W. (1999) Primordial noble gases from Earth's mantle: identification of a primitive volatile
722 component. *Science (80-.).* **285**, 2115–2118.

723 Cartwright I., Weaver T., Tweed S., Ahearne D., Cooper M., Czapnik K. and Tranter J. (2002) Stable
724 isotope geochemistry of cold CO2-bearing mineral spring waters, Daylesford, Victoria,
725 Australia: Sources of gas and water and links with waning volcanism. *Chem. Geol.* **185**, 71–91.

726 Cas R. A. F., van Otterloo J., Blaikie T. N. and van den Hove J. (2017) The dynamics of a very large
727 intra-plate continental basaltic volcanic province, the Newer Volcanics Province, SE Australia,
728 and implications for other provinces. *Geol. Soc. London, Spec. Publ.* **446**, 123–172.

729 Cayley R. A., Korsch R. J., Moore D. H., Costelloe R. D., Nakamura A., Willman C. E., Rawling T. J.,
730 Morand V. J., Skladzien P. B. and O'Shea P. J. (2011) Crustal architecture of central Victoria:
731 Results from the 2006 deep crustal reflection seismic survey. *Aust. J. Earth Sci.* **58**, 113–156.

732 Chivas A. R. ., Barnes I. E. ., Lupton J. E. . and Collerson K. (1983) Isotopic studies of south-east
733 Australian CO2 discharges. *Geol. Soc. Aust. Abstr.* **12**, 94–95.

734 Chivas A. R., Barnes I., Evans W. C., Lupton J. E. and Stone J. O. (1987) Liquid carbon dioxide of
735 magmatic origin and its role in volcanic eruptions. *Nature* **326**, 587–589.

736 Clennell M. Ben (1997) Tortuosity: a guide through the maze. *Geol. Soc. London, Spec. Publ.* **122**,
737 299–344.

738 Coulson A. (1933) The older volcanic and Tertiary marine beds at Curlewis, near Geelong. *Proc. R.*

739 *Soc. Victoria* **45**, 140–149.

740 Cox S. F., Sun S. S., Etheridge M. A., Wall V. J. and Potter T. F. (1995) Structural and geochemical
741 controls on the development of turbidite- hosted gold quartz vein deposits, Wattle Gully mine,
742 central Victoria, Australia. *Econ. Geol.* **90**, 1722–1746.

743 Craig H. (1978) A mantle helium component in circum-Pacific volcanic gases: Hakone, the Marianas
744 and Mt. Lassen. *Terriestrial Rare Gases*, 3–16.

745 Craig H. and Lupton J. E. (1976) Primordial neon, helium, and hydrogen in oceanic basalts. *Earth*
746 *Planet. Sci. Lett.* **31**, 369–385.

747 Crossey L. J., Karlstrom K. E., Springer A. E., Newell D., Hilton D. R. and Fischer T. (2009) Degassing of
748 mantle-derived CO2 and He from springs in the southern Colorado Plateau region - Neotectonic
749 connections and implications for groundwater systems. *Bull. Geol. Soc. Am.* **121**, 1034–1053.

750 Crovetto R., Fernández-Prini R. and Japas M. L. (1982) Solubilities of inert gases and methane in H_2O
751 and in D_2O in the temperature range of 300 to 600 K. *J. Chem. Phys.* **76**, 1077–1086.

752 Dahlhaus (2003) *The Dell, Clifton Springs. 3-dimensional geological model*., Available at:
753 http://www.ccmaknowledgebase.vic.gov.au/soilhealth/soils_resource_details.php?resource_id
754 =2416.

755 Darrah T. H., Vengosh A., Jackson R. B., Warner N. R. and Poreda R. J. (2014) Noble gases identify the
756 mechanisms of fugitive gas contamination in drinking-water wells overlying the Marcellus and
757 Barnett Shales. *Proc. Natl. Acad. Sci.* **111**, 14076–14081.

758 Davies D. R. and Rawlinson N. (2014) On the origin of recent intraplate volcanism in Australia.
759 *Geology* **42**, 1031–1034.

760 Deines P., Langmuir D. and Harmon R. S. (1974) Stable carbon isotope ratios and the existence of a
761 gas phase in the evolution of carbonate ground waters. *Geochim. Cosmochim. Acta* **38**, 1147–
762 1164.

763 Demidjuk Z., Turner S., Sandiford M., George R., Foden J. and Etheridge M. (2007) U-series isotope
764 and geodynamic constraints on mantle melting processes beneath the Newer Volcanic Province
765 in South Australia. *Earth Planet. Sci. Lett.* **261**, 517–533.

766 Dixon T., McCoy S. T. and Havercroft I. (2015) Legal and Regulatory Developments on CCS. *Int. J.*
767 *Greenh. Gas Control* **40**, 431–448.

768 Duddy I. R. (1997) Focussing exploration in the Otway Basin: understanding timing of source rock
769 maturation. *APPEA J.* **37**, 178–191.

770 Giese R., Henninges J., Lüth S., Morozova D., Schmidt-Hattenberger C., Würdemann H., Zimmer M.,
771 Cosma C. and Juhlin C. (2009) Monitoring at the CO2 SINK site: A concept integrating
772 geophysics, geochemistry and microbiology. *Energy Procedia* **1**, 2251–2259.

773 Giggenbach W. F., Sano Y. and Wakita H. (1993) Isotopic composition of helium, and CO2 and CH4
774 contents in gases produced along the New Zealand part of a convergent plate boundary.
775 *Geochim. Cosmochim. Acta* **57**, 3427–3455.

776 Gilfillan S., Haszedline S., Stuart F., Gyore D., Kilgallon R. and Wilkinson M. (2014) The application of
777 noble gases and carbon stable isotopes in tracing the fate, migration and storage of CO2.
778 *Energy Procedia* **63**, 4123–4133.

779 Gilfillan S. M. V., Sherk G. W., Poreda R. J. and Haszeldine R. S. (2017) Using noble gas fingerprints at
780 the Kerr Farm to assess CO2 leakage allegations linked to the Weyburn-Midale CO2 monitoring
781 and storage project. *Int. J. Greenh. Gas Control* **63**, 215–225.

782 Gilfillan S. M. V, Ballentine C. J., Holland G., Blagburn D., Lollar B. S., Stevens S., Schoell M. and
783 Cassidy M. (2008) The noble gas geochemistry of natural CO2 gas reservoirs from the Colorado
784 Plateau and Rocky Mountain provinces, USA. *Geochim. Cosmochim. Acta* **72**, 1174–1198.

785 Gilfillan S. M. V, Lollar B. S., Holland G., Blagburn D., Stevens S., Schoell M., Cassidy M., Ding Z., Zhou
786 Z., Lacrampe-Couloume G. and Ballentine C. J. (2009) Solubility trapping in formation water as
787 dominant CO(2) sink in natural gas fields. *Nature* **458**, 614–618.

788 Györe D., Gilfillan S. M. V. and Stuart F. M. (2017) Tracking the interaction between injected CO2 and
789 reservoir fluids using noble gas isotopes in an analogue of large-scale carbon capture and
790 storage. *Appl. Geochemistry* **78**, 116–128.

791 Györe D., Stuart F. M., Gilfillan S. M. V and Waldron S. (2015) Tracing injected CO2 in the Cranfield
792 enhanced oil recovery field (MS, USA) using He, Ne and Ar isotopes. *Int. J. Greenh. Gas Control*
793 **42**, 554–561.

794 Hand M. and Sandiford M. (1999) Intraplate deformation in central Australia, the link between
795 subsidence and fault reactivation. *Tectonophysics* **305**, 121–140.

796 Haszeldine R. S., Quinn O., England G., Wilkinson M., Shipton Z. K., Evans J. P., Heath J., Crossey L.,
797 Ballentine C. J. and Graham C. M. (2005) Natural geochemical analogues for carbon dioxide

storage in deep geological porous reservoirs, a United Kingdom perspective. *Oil Gas Sci. Technol.* **60**, 33–49.

Holland G. and Gilfillan S. (2013) Application of noble gases to the viability of CO2storage. In *The Noble Gases as Geochemical Tracers* Springer Berlin Heidelberg, Berlin, Heidelberg. pp. 177–223.

IPCC (2005) *IPCC Special report on Carbon Dioxide Capture and Storage*., UK: Cambridge University Press, New York. Available at: https://www.ipcc.ch/pdf/special-reports/srccs/srccs_wholereport.pdf.

Italiano F., Yuce G., Uysal I. T., Gasparon M. and Morelli G. (2014) Insights into mantle-type volatiles contribution from dissolved gases in artesian waters of the Great Artesian Basin, Australia. *Chem. Geol.* **378**–**379**, 75–88.

Jeandel E., Battani A. and Sarda P. (2010) Lessons learned from natural and industrial analogues for storage of carbon dioxide. *Int. J. Greenh. Gas Control* **4**, 890–909.

Karolytė R., Serno S., Johnson G. and Gilfillan S. M. V. (2017) The influence of oxygen isotope exchange between CO2 and H2O in natural CO2-rich spring waters: Implications for geothermometry. *Appl. Geochemistry* **84**, 173–186.

King S. D. and Anderson D. L. (1998) Edge-driven convection. *Earth Planet. Sci. Lett.* **160**, 289–296.

Kipfer R., Aeschbach-Hertig W., Peeters F. and Stute M. 4 Noble Gases in Lakes and Ground Waters.

Kipfer R., Aeschbach-Hertig W., Peeters F. and Stute M. (2002) Noble Gases in Lakes and Ground Waters. *Rev. Mineral. Geochemistry* **47**, 615–700.

Lawrence C. R. (1969) Hydrogeology of the Daylesford Mineral District with special reference to the mineral springs. *Geol. Surv. Victoria, Undergr. water Investig. Rep.* **12**.

Lesti C., Giordano G., Salvini F. and Cas R. (2008) Volcano tectonic setting of the intraplate, Pliocene-Holocene, Newer Volcanic Province (southeast Australia): Role of crustal fracture zones. *J. Geophys. Res. Solid Earth* **113**, 1–11.

Liu W., Tao C., Borjigin T., Wang J., Yang H., Wang P., Luo H. and Zhai C. (2016) Formation time of gas reservoir constrained by the time-accumulation effect of 4He: Case study of the Puguang gas reservoir. *Chem. Geol.* **469**, 246–251.

Lyon, Boult P. J., Watson M. N. and Hillis R. (2005) A systematic fault seal evaluation of the Ladbroke

827 Grove and Pyrus traps of the Penold Trough, Otway Basin. *Aust. Pet. Prod. Explor. Assoc. J.* **45**,
828 459–476.

829 Mao X., Wang Y., Chudaev O. V. and Wang X. (2009) Geochemical evidence of gas sources of CO2-
830 rich cold springs from Wudalianchi, Northeast China. *J. Earth Sci.* **20**, 959–970.

831 Marty B. and Jambon A. (1987) C3He in volatile fluxes from the solid Earth: implications for carbon
832 geodynamics. *Earth Planet. Sci. Lett.* **83**, 16–26.

833 Marty B. and Tolstikhin I. N. (1998) CO2 fluxes from mid-ocean ridges, arcs and plumes. *Chem. Geol.*
834 **145**, 233–248.

835 Matthews A., Fouillac C., Hill R., O'Nions R. K. and Oxburgh E. R. (1987) Mantle-derived volatiles in
836 continental crust: the Massif Central of France. *Earth Planet. Sci. Lett.* **85**, 117–128.

837 Myers M., Stalker L., Pejcic B. and Ross A. (2013) Tracers – Past, present and future applications in
838 CO2 geosequestration. *Appl. Geochemistry* **30**, 125–135.

839 Newell D. L., Jessup M. J., Hilton D. R., Shaw C. A. and Hughes C. A. (2015) Mantle-derived helium in
840 hot springs of the Cordillera Blanca, Peru: Implications for mantle-to-crust fluid transfer in a
841 flat-slab subduction setting. *Chem. Geol.* **417**, 200–209.

842 O'Nions R. K. and Oxburgh E. R. (1988) Helium, volatile fluxes and the development of continental
843 crust. *Earth Planet. Sci. Lett.* **90**, 331–347.

844 van Otterloo J., Cas R. A. F. and Sheard M. J. (2013) Eruption processes and deposit characteristics at
845 the monogenetic Mt. Gambier Volcanic Complex, SE Australia: implications for alternating
846 magmatic and phreatomagmatic activity. *Bull. Volcanol.* **75**, 737.

847 van Otterloo J., Raveggi M., Cas R. A. F. and Maas R. (2014) Polymagmatic Activity at the
848 Monogenetic Mt Gambier Volcanic Complex in the Newer Volcanics Province, SE Australia: New
849 Insights into the Occurrence of Intraplate Volcanic Activity in Australia. *J. Petrol.* **55**, 1317–
850 1351.

851 Ozima M. and Podosek F. A. (2002) *Noble Gas Geochemistry*., Cambridge University Press.

852 Price R. C., Gray C. M. and Frey F. A. (1997) Strontium isotopic and trace element heterogeneity in
853 the plains basalts of the Newer Volcanic Province, Victoria, Australia. *Geochim. Cosmochim.*
854 *Acta* **61**, 171–192.

855 Roberts J. J., Gilfillan S. M. V., Stalker L. and Naylor M. (2017) Geochemical tracers for monitoring

offshore CO2 stores. *Int. J. Greenh. Gas Control* **65**, 218–234.

Robertson G. B., Prescott J. R. and Hutton J. T. (1996) Thermoluminescence dating of volcanic activity at Mount Gambier, South Australia. *Trans. R. Soc. South Aust.* **120**, 7–12.

Rudnick R. L. and Fountain D. M. (1995) Nature and composition of the continental crust: A lower-crustal perspective. *Rev. Geophys.* **33**, 267–309.

Ruzié L., Aubaud C., Moreira M., Agrinier P., Dessert C., Gréau C. and Crispi O. (2013) Carbon and helium isotopes in thermal springs of La Soufrière volcano (Guadeloupe, Lesser Antilles): Implications for volcanological monitoring. *Chem. Geol.* **359**, 70–80.

Sakamoto M., Sano Y. and Wakita H. (1992) 3He/4He ratio distribution in and around the Hakone volcano. *Geochem. J.* **26**, 189–195.

Sano Y. and Marty B. (1995) Origin of carbon in fumarolic gas from island arcs. *Chem. Geol.* **119**, 265–274.

Sano Y., Takahata N. and Seno T. (2006) Geographical distribution of 3He/4He ratios in the Chugoku District, Southwestern Japan. *Pure Appl. Geophys.* **163**, 745–757.

Sano Y., Wakita H. and Williams S. N. (1990) Helium-isotope systematics at Nevado del Ruiz volcano, Colombia: implications for the volcanic hydrothermal system. *J. Volcanol. Geotherm. Res.* **42**, 41–52.

Sherwood Lollar B., Ballentine C. J. and O'Nions R. K. (1997) The fate of mantle-derived carbon in a continental sedimentary basin: Integration of relationships and stable isotope signatures. *Geochim. Cosmochim. Acta* **61**, 2295–2307.

Sherwood Lollar B., O'Nions R. K. and Ballentine C. J. (1994) Helium and neon isotope systematics in carbon dioxide-rich and hydrocarbon-rich gas reservoirs. *Geochim. Cosmochim. Acta* **58**, 5279–5290.

Shugg A. (2009) Hepburn Spa: Cold carbonated mineral waters of Central Victoria, South Eastern Australia. *Environ. Geol.* **58**, 1663–1673.

Smith S. P. (1985) Noble gas solubility in water at high temperature. *Eos (Washington. DC).* **66**, 397.

Stalker L. and Myers M. (2014) Tracers–pilot versus commercial scale deployment for carbon storage. *Energy Procedia* **63**, 4199–4208.

884 Teasdale J. P., Pryer L. L., Stuart-Smith P. G., Romine K. K., Etheridge M. A., Loutit T. S. and Kyan D.
885 M. (2003) Structural framework and basin evolution of Australia's southern margin. *APPEA J.*
886 **43**, 13–37.

887 Tolstikhin I. N., Ballentine C. J., Polyak B. G., Prasolov E. M. and Kikvadze O. E. (2017) The noble gas
888 isotope record of hydrocarbon field formation time scales. *Chem. Geol.* **471**, 141–152.

889 Torgersen T. (1980) Controls on pore-fluid concentration of 4He and 222Rn and the calculation of
890 4He/222Rn ages. *J. Geochemical Explor.* **13**, 57–75.

891 Walton N. R. G. (1989) Electrical conductivity and Total Dissolved Solids—what is their precise
892 relationship? *Desalination* **72**, 275–292.

893 Watson M. N., Boreham C. J. and Tingate P. R. (2004) Carbon dioxide and carbonate cements in the
894 Otway Basin; implications for geological storage of carbon dioxide. *APPEA J.* **44**, 703–720.

895 Watson M. N., Zwingmann N., Lemon N. M. and Tingate P. R. (2003) Onshore Otway Basin carbon
896 dioxide accumulations: CO2-induced diagenesis in natural analogues for underground storage
897 of greenhouse gas. *APPEA J.* **43**, 637–653.

898 Wellman P. (1983) Hotspot volcanism in Australia and New Zealand: Cainozoic and mid-Mesozoic.
899 *Tectonophysics* **96**, 225–243.

900 Wellman P. and McDougall I. (1974) Cainozoic igneous activity in eastern Australia. *Tectonophysics*
901 **23**, 49–65.

902 Wilkinson M., Gilfillan S. M. V, Haszeldine R. S. and Ballentine C. J. (2009) Plumbing the Depths:
903 Testing Natural Tracers of Subsurface CO2 Origin and Migration, Utah. In *Carbon dioxide*
904 *sequestration in geological media-State of the science* AAPG Special Volumes. pp. 619–634.

905 Williams S. N., Sano Y. and Wakita H. (1987) Helium-3 emission from Nevado Del Ruiz Volcano,
906 Colombia. *Geophys. Res. Lett.* **14**, 1035–1038.

907 Wycherley H., Fleet A. and Shaw H. (1999) Some observations on the origins of large volumes of
908 carbon dioxide accumulations in sedimentary basins. *Mar. Pet. Geol.* **16**, 489–494.

909 Zhou Z. and Ballentine C. J. (2006) 4He dating of groundwater associated with hydrocarbon
910 reservoirs. *Chem. Geol.* **226**, 309–327.

911